UC Santa Barbara
UC Santa Barbara Electronic Theses and Dissertations

Title

Appendage Regeneration in the Primitive Chordate Ciona Robusta

Permalink

https://escholarship.org/uc/item/4mz7m55j

Author

Spina, Elijah James

Publication Date

2017

Peer reviewed|Thesis/dissertation

UNIVERSITY OF CALIFORNIA

Santa Barbara

Appendage Regeneration in the Primitive Chordate *Ciona Robusta*

A dissertation submitted in partial satisfaction of the

requirements for the degree Doctor of Philosophy

in Molecular, Cellular and Developmental Biology

by

Elijah James Spina

Committee in charge:

Professor William C. Smith, Chair

Professor Dennis O. Clegg

Professor Anthony W. De Tomaso

Professor Denise J. Montell

September 2017

The dissertation of Elijah James Spina is approved.

_____

Dennis O. Clegg

_____

Anthony W. De Tomaso

_____

Denise J. Montell

_____

William C. Smith, Committee Chair

August 2017

Appendage Regeneration in the Primitive Chordate *Ciona Robusta*

ACKNOWLEDGEMENTS

VITA OF ELIJAH JAMES SPINA

Education

Ph.D. Molecular, Cellular & Developmental Biology (Expected Aug. 2017)
University of California, Santa Barbara (UCSB)
B.S. Biological Sciences (2009)
State University of New York at Oneonta (SUNY Oneonta)

Work Experience

UCSB, Santa Barbara, California (2011 – 2017)
- Doctoral Researcher and Instructor
- Teaching assistant for capstone course in Cell & Developmental Biology emphasis (Fall & Winter 2013-2017)

Columbia University Medical Center, New York, NY (2010 – 2011)
- Laboratory Technician
- Performed essential wet lab research for clinical trials pertaining to endocrinology, bone homeostasis, osteoporosis and diabetes.

New Hope Fertility Center, New York, NY (2009 – 2010)
- Consultant
- Successfully revised internal system of reporting in-vitro fertilization (IVF) patient outcomes and established a standard operating procedure for reporting to the CDC.

Leadership Development
- UCSB Graduate Biology Mentorship Association, President & Event Coordinator (05/2014 – 06/2017)
- The Leadership Challenge® (UCSB Fall 2016)
- Mentor for UCSB CAMP undergraduate diversity research scholarship (2013)

Publications, Awards & Presentations
- E.J. Spina, E.B. Guzman, H. Zhou, K.S. Kosik, W.C. Smith. " A microRNA-mRNA Expression Network during Oral Siphon Regeneration in Ciona" Development (2017)
- E.J. Spina, T.T.H. Nguyen, E.B. Guzman, H. Zhou, K.S. Kosik, W.C. Smith, "microRNA Regulation of Oral Siphon Regeneration In *Ciona intestinalis*" (2014 EMBO Conference on the Molecular and Cellular Basis of Regeneration)
- NIGMS; UC Irvine, CCBS, NSCSB Graduate Student Fellowship (2014)
- UCSB, MCDB/Amgen Teaching-Research Fellowship (09/2011 – 07/2012)
- SUNY Oneonta Magna cum laude with Honors in Biology (2009)
- Bennett, Jacqueline S., Kaitlyn L. Charles, Matthew R. Miner, Caitlin F. Heuberger, Elijah J. Spina, Michael F. Bartels, and Taylor Foreman. "Ethyl lactate as a tunable solvent for the synthesis of aryl aldimines." Green Chemistry 11 (2009): 166-68.
- SUNY Oneonta Student Grant for Research and Creative Activity (2008)

ABSTRACT

Appendage Regeneration in the Primitive Chordate *Ciona Robusta*

by

Elijah James Spina

Here I present a parallel study of mRNA and microRNA expression during oral siphon

(OS) regeneration in *Ciona robusta*, and the derived network of their interactions. In the

process of identifying 248 mRNAs and 15 microRNAs as differentially expressed, I also

identified 57 novel microRNAs, several of which are among the most highly differentially

expressed. Analysis of functional categories identified enriched transcripts related to stress

responses and apoptosis at the wound healing stage, signaling pathways including Wnt and

TGFβ during early regrowth, and negative regulation of extracellular proteases in late stage

regeneration. Consistent with the expression results, I found that inhibition of TGFβ

signaling blocked OS regeneration.

A correlation network was subsequently inferred for all predicted microRNA-mRNA

target pairs expressed during regeneration. Network-based clustering associated transcripts

into 22 non-overlapping groups, then functional analysis of network clusters showed

enrichment of stress response, signaling pathway and extracellular protease categories could

be related to specific microRNAs. Predicted targets of the miR-9 cluster suggest a role in

regulating differentiation and the proliferative state of neural progenitors through regulation of the cytoskeleton and cell cycle.

Additional experiments were performed to identify precursor cells which contribute to OS regeneration. A population of cells expressing the pluripotency marker Piwi (was observed to accumulate at the distal edge of regenerating OS blastemas, suggesting they may act as multi- or pluri-potent stem cells which contribute to siphon regeneration by differentiating into the functional tissues. Another population of Piwi expressing cells (PECs) has been identified in the transverse vessels of the branchial sac and these cells appear to increase in number following OS amputation. Expansion of the branchial sac (BS) PEC population following amputation could be inhibited by several pharmacological inhibitors of major conserved signaling pathways that I identified in the above-mentioned RNAseq study. This observation supports the hypothesis that signaling occurring within the regenerating OS is capable of inducing expansion of the PEC population in the BS, likely through the action of circulating PECs. However, the function of PECs and contribution to siphon regeneration remains unresolved.

TABLE OF CONTENTS

LIST OF FIGURES

I. History and Scope of Regeneration Research

Records of human fascination with animal regeneration date back to ancient Greece. Tales of the mythical hydra, a beast that regrew two heads each time it was decapitated, and the regenerating liver of Prometheus illustrate this cultures' reverence for this apparently immortalizing trait. Scientific study began with observations by Aristotle that lizards could regenerate their tail; however the first journal article about regeneration was not published until nearly two millennia later in 1712 (Odelberg, 2004). Despite longstanding interest, the field of regeneration has proceeded rather slowly because of a lack of adequate tools to address key mechanistic questions. Thomas Morgan synthesized a thorough review of the literature in his 1901 paper, however, it wasn't until advancements in molecular biology in the latter half of the 20th century that we began to understand how or why some animal species can regenerate well, but others cannot (Maienschein, 2011).

I.A. Regeneration is an Ancient Survival Strategy in Animals

The ability of metazoan animals to regenerate varies widely and is distributed throughout the kingdom (Fig 1). The ability to regenerate lost tissues can be interpreted as a spectrum extending from extreme cases of whole body regeneration, such as is observed in planaria (Reddien and Sánchez Alvarado, 2004) and colonial ascidians (Rinkevich et al., 1995, 2010; Zondag et al., 2016), to cases of limited cell replacement
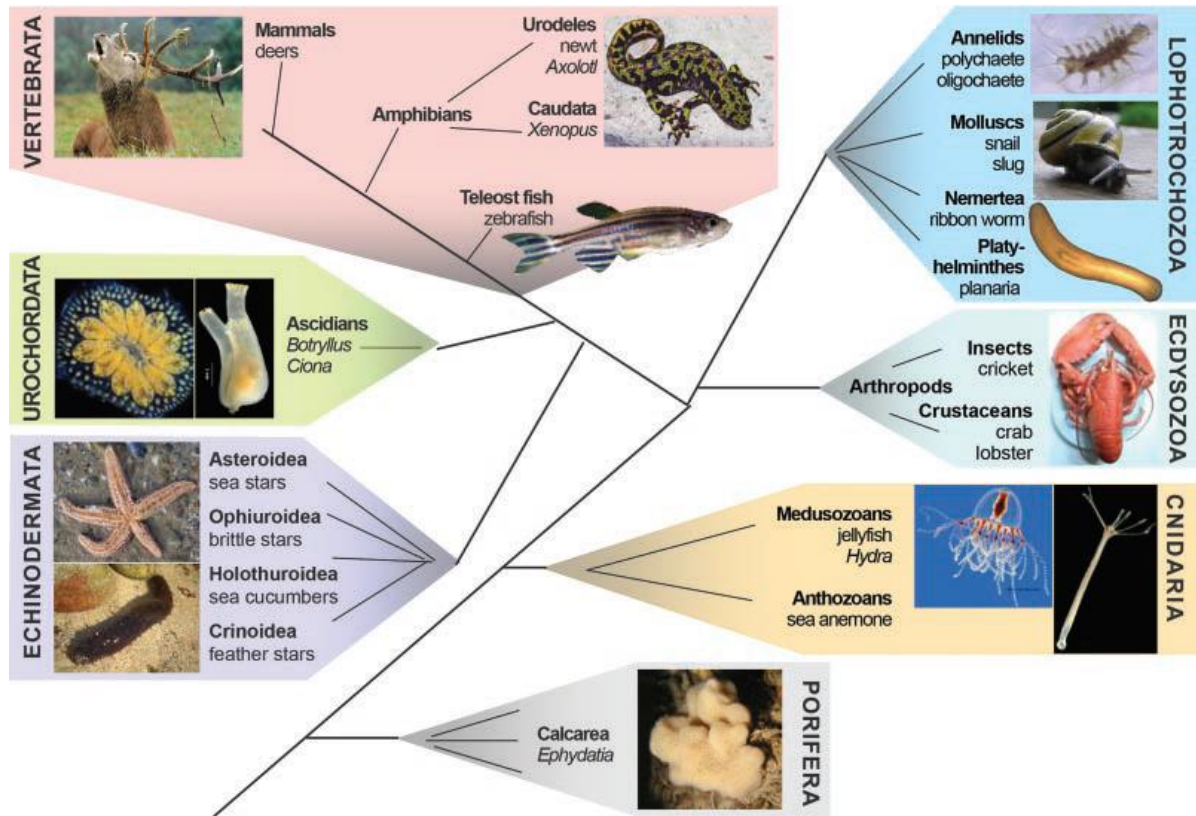
Figure 1. Distribution of regenerative potential across the animal kingdom. This diagram shows a phylogenetic tree of the animal species exhibiting regenerative potential after injury. Reproduced with permission from Galliot and Ghila, (2010).

during tissue homeostasis, such as is observed in the mammalian digestive tract (Barker, 2014; Barker et al., 2008) .

In addition, many species display regenerative capacities that vary with life stage and injury severity (Rinkevich et al., 2013). Most vertebrates, including humans, heal wounds using fibrotic mechanisms that inhibit subsequent tissue regrowth by leaving dense connective tissue which prevents regeneration to the original functional state (Harty et al., 2003). By contrast, there are several well characterized examples of vertebrates that are able to replace whole organs and/or appendages composed of multiple

tissue types (King and Newmark, 2012; Stoick-Cooper et al., 2007). Furthermore, differences in cellular responses appear to directly underlie the differences in regenerative capacity of various organisms, as evidenced by differences in scar formation between regenerating vertebrates (e.g., salamanders) and non-regenerating vertebrates (Seifert et al., 2012).

Comparative studies of development have identified numerous conserved aspects of embryo formation and morphogenesis; however, there also seem to be many developmental features which are taxa specific. The process of animal development can be summarized in stages proceeding from cleavage, to gastrulation, neurulation and ultimately morphogenesis and organ formation. Regeneration has been summarized in an analogous manner; proceeding from wound healing, mobilization of precursors then finally to morphogenesis and restoration of homeostasis (Fig 2). Several events in each stage of regeneration appear to have parallels across model systems used to study regeneration, however the discovery of several taxa-specific features (such as Prod-1 signaling in salamanders) have created confusion regarding the evolutionary relationship between the molecular and cellular regulators that coordinate regeneration in these different systems (Geng et al., 2015; da Silva et al., 2002). Despite the presence of various non-conserved cell types and utilization of both conserved and non-conserved signaling mechanisms in diverse ways, there is extensive evidence that developmental processes are highly conserved. A similar logic can be applied to the hypothesis that regeneration is a conserved process.
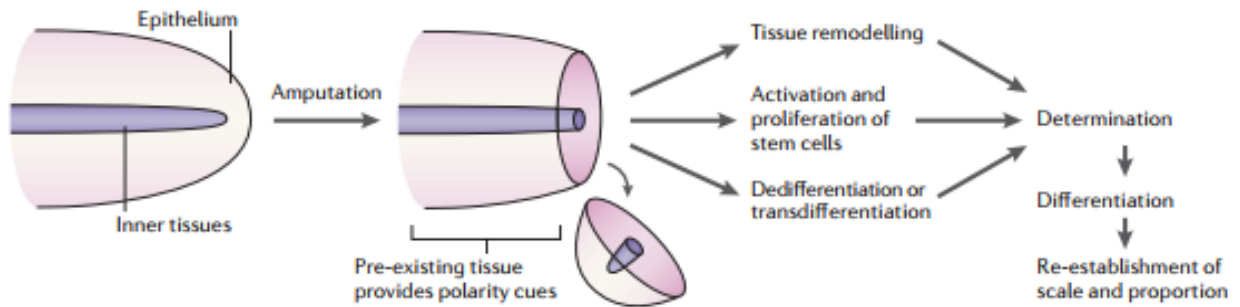
Figure 2 | Basic mechanisms of regeneration. After amputation, wound healing occurs. This is an injury response that is common to all animals, whether or not they can regenerate. After wound healing, if the resulting tissue stump is capable of regeneration, at least three processes can be activated, either independently or together. Hydra, for example, undergoes remodeling of pre-existing tissues to regenerate amputated parts. Planarians undergo both tissue remodeling and proliferation of resident adult somatic stem cells; in vertebrates, both stem-cell proliferation and the dedifferentiation or trans-differentiation of the cells that lie adjacent to the plane of amputation take place. The cells that respond to the stimulus of amputation eventually undergo determination and differentiation, resulting in new tissues that must then functionally integrate with and scale to the size of the pre-existing tissues. Reproduced with permission from (Alvarado and Tsonis, 2006).

The observation that regeneration proceeds through similar stages in all systems studied (Fig 1), and that regeneration employs both conserved and non-conserved developmental signaling mechanisms specific to each taxa, suggests the reason some animals do not regenerate well is that evolutionary loss of this trait has occurred in those lineages as a trade-off for increased fitness (Bely and Nyberg, 2010; Tiozzo and Copley, 2015). Therefore, regeneration is likely an ancestral animal trait which has been selectively maintained to improve survival within particular taxa. By identifying points of evolutionary conservation and divergence in the molecular mechanisms underlying regeneration, progress can be made

toward illuminating how different species can accomplish the same task in vastly different ways (Fig 2).

.I.B. Divergent Cellular and Molecular Mechanisms of Regeneration

A commonly observed feature in animal regeneration is the formation of a blastema, which is loosely defined as a mass of mesenchymal-like cells that forms shortly after wound healing at the distal tip of a regenerating appendage and subsequently proliferates to reform new tissues. In salamanders, the limb blastema is composed primarily of a local population of dermal fibroblasts which maintain plasticity to differentiate into a limited subset of cell types, while the remaining cells are comprised of lineage-restricted progenitors which can generally regenerate tissues only within their respective tissue types (Kragl et al., 2009; Satoh et al., 2008). This is in contrast to cellular progenitors in flatworm regeneration, where pluripotent stem cells called neoblasts migrate to the site of the wound and differentiate to form progeny representing all three germ layers(Guedelhoefer and Sánchez Alvarado, 2012; Wagner et al.,

Table 1. Conserved Signaling Pathways Involved in Cellular Differentiation

Signaling Pathway	Species/Group		
	Hydra	Planaria	Vertebrates
TGF-β	Yes	Yes	Yes
Notch	Yes	Yes	Yes
Wingless (Wnt)	Yes	Yes	Yes
Hedgehog	Yes	Yes	Yes
JAK/STAT	Unknown	Yes	Yes
EGF	Yes	Yes	Yes
FGF	Yes	Yes	Yes
Toll/NF-κβ	Unknown	Yes	Yes

Modified from Galliot and Ghila, (2010).

2011).

Several conserved signaling pathways are used to initiate and coordinate the process of regeneration (Table 1); however, the context of how and when each signal is deployed is widely divergent. Probably the most studied example is Wnt signaling, which seems to be required for recruiting progenitor cells as well as initiating proliferation of blastema cells in salamanders, but it also plays a role in determining A/P polarity during planaria regeneration (Whyte et al., 2012). There is also a conserved requirement for the presence of nerves at the site of injury during the recruitment of blastemal cells. However, the molecules which comprise these signals remain largely elusive (Kumar and Brockes, 2012; Monaghan et al., 2009)

II. Regeneration in Ascidians

Ascidians are members of the chordate sub-phylum Tunicata and are the closest extant relatives of the vertebrates (Delsuc et al., 2006). Studies of regeneration in these animals began over 125 years ago with observations that individuals could regenerate after amputation of the neural complex or siphons. Due to conflicting reports supporting claims of Lamarckism there was a period of relative inactivity in the field of *Ciona* regeneration research when one scientist claimed amputation of the *Ciona* OS resulted in regeneration of a longer siphon that was inherited by the next generation. It wasn't until 1975 that additional experiments were published demonstrating the falsity of those

previous claims. Recently, work on *Ciona* regeneration has advanced rapidly led by several studied published by Dr. William Jeffery and colleagues. These recent efforts laid the foundation for my work presented here.

II.A. Ascidian Life-Histories and Reproductive Strategies

Regenerative ability is highly variable among the vertebrates and whole-organ regeneration is limited to very few species. However, tunicates show robust regenerative abilities. Ascidians tend to display indeterminate growth, where the majority of tissues continue to grow throughout an individual's life, yet the connection between indeterminate growth and stem cell turnover during regeneration remains largely unexplored (Vogt, 2012). Tunicates appear to have diverged before two whole-genome duplications that are speculated to have occurred at the origin of the vertebrate lineage (Dehal and Boore, 2005), and are thought to have subsequently evolved towards reduced morphological and genomic complexity (Crow and Wagner, 2006). These traits in combination with a sequenced and well-annotated genomes make the tunicate powerful models for identifying the components and interactions which comprise gene regulatory networks that govern biological processes, including regeneration (Dehal et al., 2002; Satou et al., 2008).

The colonial ascidians, such as *Botryllus schlosseri* (Fig 3A), show whole body regeneration (Kürn et al., 2011; Rinkevich et al., 1995; Voskoboynik et al., 2007). *Ciona intestinalis* and *Ciona robusta* (Fig 3B), two species that

7
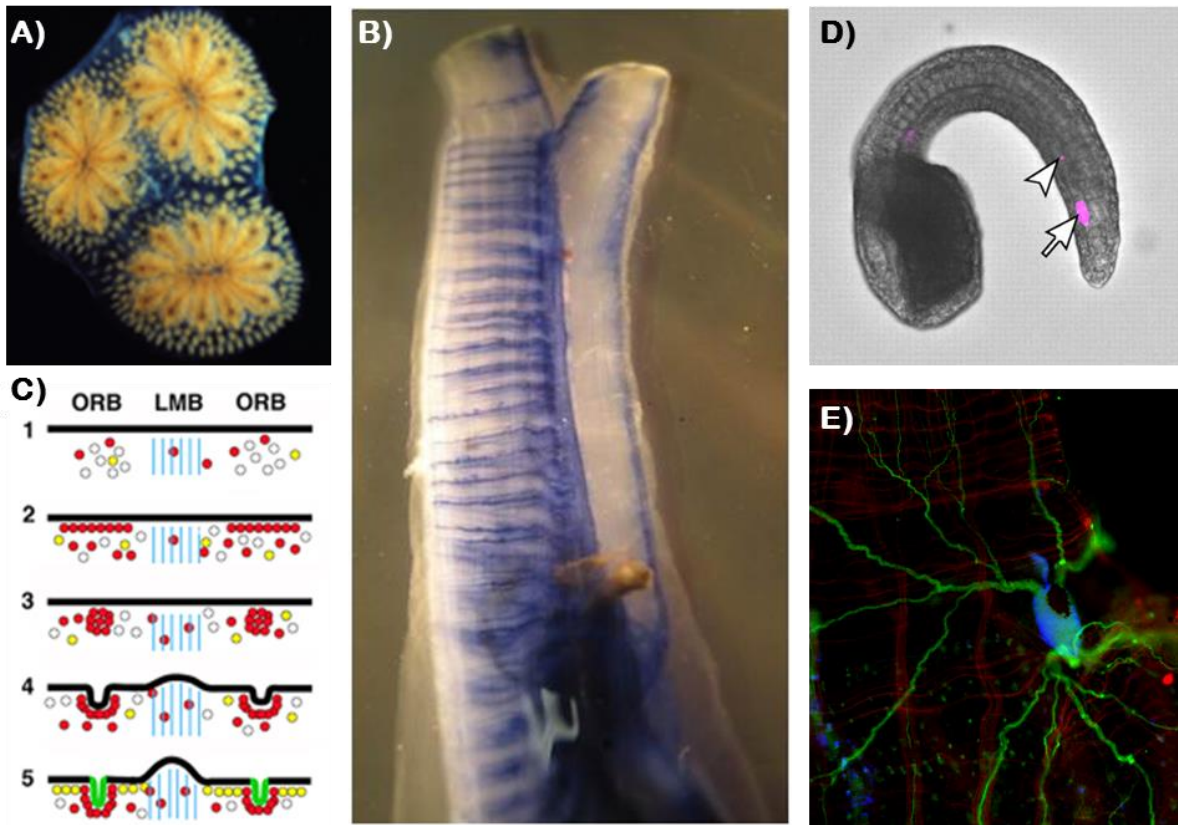
Figure 3. Regenerative Tissues in Ascidians. A) *B. schlosseri* is a colonial ascidian that displays whole-body regenerative capacity (image courtesy of Dr. Anthony De Tomaso), B) An adult *C. robusta* with the vasculature stained by trypan blue, C) Diagram depicting the five stages of oral siphon pigment organ regeneration along the oral siphon (thick black horizontal line) in young animals. ORB: oral siphon regeneration bands. LMB: longitundinal muscle bands. Open circle: undifferentiated cells. Red circles: red pigment cells, yellow circles: yellow pigment cells. Blue horizontal lines: longitundinal muscle fibers. From (Jeffery, 2012), D) A *Ciona* tailbud embryo showing lineage traced B8.11 (arrowhead) and B8.12 (arrow) cells in the tail labeled by DiI. From (Shirae-Kurabayashi et al., 2006), E) The CNS of a juvenile *C. robusta* labeled using DAPI (blue) and B-Tubulin (green), with the musculature labeled by actin/phalloidin staining (red).

until recently were both called *Ciona intestinalis* (Brunetti et al., 2015), are well established models for embryology. When they become post-metamorphic adults, *Ciona* can rapidly and robustly regenerate several tissues including their siphons (Fig 3C), primordial germ cells (Fig 3D), and central nervous system (Fig 3E) (Jeffery, 2015a). The oral siphon (OS) is a

cylindrical appendage composed primarily of muscular tissue, vasculature, nerves, epidermis, eight oral pigment organs located at the distal tip (Fig 3C), and an outer coating of tunic (Chiba et al., 2004).

II.B. Germline Regeneration in Ascidians

Germline cells face strong selective pressure to maintain the integrity of an organism's genome, meaning that they must maintain the information they received and transmit that information faithfully to the next generation with high fidelity. While somatic cells maintain the germline niche, they are typically segregated early during embryogenesis in many common model organisms. However, post-embryonic germline segregation may actually be the ancestral mechanism, where long term multipotent progenitors are established in the embryo from which the germline is segregated later in life (Juliano and Wessel, 2010). This segregation is partially accomplished because the DNA of germline cells is maintained in a hypo-methylated state, while somatic cells typically undergo progressive methylation during differentiation (Huang and Fan, 2010; Messerschmidt et al., 2014).

Germline cells are often characterized by high levels of expression of genes that are also highly expressed in mammalian pluripotent stem cells such as Piwi and Nanos (Juliano and Wessel, 2010). Piwi is a member of the Argonaute family of proteins which associate with a specific class of small

RNA, piRNAs and function together in a ribonucleoprotein complex to repress transposon transcription. Silencing transposons is important for protecting the integrity of a genome because transposon activity (particularly re-insertion at random sites in the host genome) can be severely disruptive to genes present at the re-insertion site. Further, the Piwi-piRNA complex is not limited to repressing transposon transcription; it can also inhibit translation by targeting mRNA directly for degradation or sequestration. Germline cells express a number of other genes that are important repressors of somatic differentiation programs, including Pem-1, PIE-1, Pgc, and Blimp-1 (Shirae-Kurabayashi et al., 2011; Weissman, 2000).

Do somatic and germline stem cells originate from a common precursor in *Ciona*? During embryonic development in *Ciona robusta*, the B7.6 cell divides into B8.11 & B8.12 lineages (Fig 3D) (Venuti and Jeffery, 1989). The RNA of two germline specific markers, Vasa & Pem-1, segregates into both B8 lineages, but Vasa protein is maintained only in the B8.12 lineage (Shirae-Kurabayashi et al., 2011). Simultaneously, the B8.11 lineage inherits three markers of somatic tissues, the so-called "post-plasm", centrosome attracting body (CAB) and Macho-1 protein; as these cells develop into the gut wall of the adult animal (Nishida and Sawada, 2001). Meanwhile, the Vasa rich B8.12 cells localize to the endodermal strand and develop into the gonad primordium.

The endodermal strand is located in the tail of *Ciona robusta* larvae. This leaves them vulnerable to injury until the animal attaches its anterior end to a substrate and undergoes metamorphosis to internalize the gonad primordium. An incredible phenomenon happens when a *Ciona* larvae suffers severe tail damage and/or amputation that destroys the Vasa+ cells residing in the endodermal strand (the B8.12 germline precursors) –these animals are able to induce the formation of a new set of Vasa+ cells apparently arising from the gut wall (Shirae-Kurabayashi et al., 2006). This evidence of a compensatory mechanism to restore normal gonads in juvenile *Ciona robusta* suggests that germline potency is maintained in the B8.11 line despite early commitment to a somatic fate. Further experiments using lineage tracing of the B8.11 line in tail-amputated *Ciona robusta* larvae would identify if they are the source of the regenerated germline cells.

II.C. Central Nervous System (CNS) Regeneration in *Ciona*

Adult *Ciona* are capable of regenerating their entire CNS after ablation by physical trauma (Dahlberg et al., 2009). The CNS is composed of two main structures; the cerebral ganglion and the dorsal strand plexus. Most of the cell bodies that compose the signal integration centers of the CNS neurons reside in the cerebral ganglion, however, neural cell bodies have also been observed in smaller ganglion-like aggregates located along peripheral nerves emanating from the cerebral ganglion. In contrast to the

cerebral ganglion, the putative composition and function of the dorsal strand plexus remains largely undescribed.

Complete ablation of the *Ciona* CNS does not affect feeding behavior as indicated by continuous filtration of water through the pharynx. However, CNS ablation does disrupt certain physiological processes such as loss of the longitudinal muscle contraction response (indicating loss of CNS sensory integration and motor response activity) during a physical touch assay where the distal tip of either siphon is gently poked by a probe (Dahlberg et al., 2009). Further, detailed observations of pan-neuronal molecular markers shows thorough innervation of the OS by nerves emanating from the cerebral ganglion, which supports the hypothesis that these neuronal connections are necessary for tactile sensory integration (Osugi et al., 2017).

II.D. Siphon Regeneration in *Ciona*

In addition to a capacity for regenerating germline progenitors and the entire CNS; adult *Ciona* can also regenerate two cylindrical appendage-like structures, known as siphons, which intake and expel water from the pharynx during feeding. The oral (incurrent) siphon is located at the most anterior end of the animal and normally contains 8 pigment spots circumscribing the distal tip. The atrial (excurrent) siphon is located toward the anterior end of the dorsal side and normally contains 6 pigment spots circumscribing the distal tip.

During *Ciona* development, cell lineages are generally specified and determined very as demonstrated by blastomere labeling, isolation and transplant experiments. The oral and atrial siphons originate from placodes, or raised patches of cells, which coalesce into a rosette-like structure prior to metamorphosis (Kourakis and Smith, 2007). The OS rosette invaginates to connect with the neurohypophyseal duct, which is the most anterior part of the *Ciona* neural tube (Veeman et al., 2010). This physical homology, along with homologous gene expression patterns, supports the hypothesis that the OS is homologous to the vertebrate mouth.

Amputation of either siphon initiates a regenerative response to replace the lost appendage, the fidelity and speed of which depends on the age and size of the animal as well as the amputation severity. Upon completion of regeneration, the new siphon is indistinguishable from the original unless the amputation also included a portion of the pharynx or occurred in an elderly animal (Jeffery, 2015b). In the two latter cases, an incorrect number of pigment spots may be present in the regenerated siphon, indicating disruption of morphological patterning signals due to the severity of the amputation or compromised regenerative capacity due to aging. Further, amputation of the entire anterior end of an adult *Ciona* (which includes both of the siphons, the CNS and a portion of the pharynx) can result in either failed regeneration (leading to death) or regeneration of two atrial siphons and one oral siphon. The regeneration of two atrial siphons during severe anterior amputations indicates a recapitulation of *Ciona* developmental

processes that normally occur after metamorphosis in which two atrial siphons initially develop on the lateral sides before fusing into a single functional siphon on the dorsal side of the animal.

The blastema formed during OS regeneration is reminiscent of those observed in other species that undergo appendage regeneration, wherein a region of proliferative cells can been observed distal edge of the amputation site (Hamada et al., 2015; Jeffery, 2015a). The distal structures of the appendage are typically reformed shortly after amputation and there is no obvious accumulation of mesenchymal cells or lack of pigmentation at the distal margin during early stages of regeneration, as has been observed in the regenerating newt limb and zebrafish fin (McCusker et al., 2015; Pfefferli and Jaźwińska, 2015). This peculiar mode of regeneration is sometimes described as intercalary growth, where the distal morphology is reformed before the interceding region becomes expanded to regenerate the new appendage to its proper size (Auger et al., 2010).

Table 2. Typical Duration of a Regeneration Experiment in Various Model Organisms

Organism	Time
Ciona	1-2 weeks
Planaria	1-2 weeks
Zebrafish	2-4 weeks
Salamander	1-2 months

Note: Times were estimated from various anecdotal sources.

III. Gene Expression during Oral Siphon Regeneration

To address why only a subset of animal species are capable of regenerating, and to address how these species might regulate the regenerative process, many studies have sought to characterize gene expression profiles of regenerating

tissues. Although the aforementioned studies have identified numerous molecular mechanisms governing cellular responses during regeneration, little is known about how various molecular events are coordinated (Endo et al., 2004; Jhamb et al., 2011; King and Newmark, 2012). This deficiency is evident in the current lack of effective molecular therapies available to stimulate tissue regeneration (Stoick-Cooper et al., 2007). The ability to detect transcript level changes in a comprehensive and unbiased manner can identify previously unknown interactions between signaling pathways, transcription factors and effector genes required for regeneration. There have been several transcriptome-wide studies of gene expression of both mRNA (Campbell et al., 2011; Hamada et al., 2015; Knapp et al., 2013; Love et al., 2011; Monaghan et al., 2009; Schebesta et al., 2006; Stewart et al., 2013; Wu et al., 2013) and microRNA (miRNA) (Gearhart et al., 2015; Holman et al., 2012; Hutchins et al., 2016; Thatcher et al., 2008) during appendage regeneration. However, none of these studies connected the expression profiles of miRNA to those of mRNA.

In the current study, I present a transcriptome-wide investigation of both mRNA and miRNA expression profiles from stage matched samples during appendage regeneration of *C. robusta* (Fig 4). I constructed a network of correlations between these two RNA types and inferred the function of miRNAs within a network based on the functions of their predicted target mRNAs. Our approach expands upon previous work by analyzing tissues both distal and proximal to the amputation plane using high-throughput RNA sequencing

15
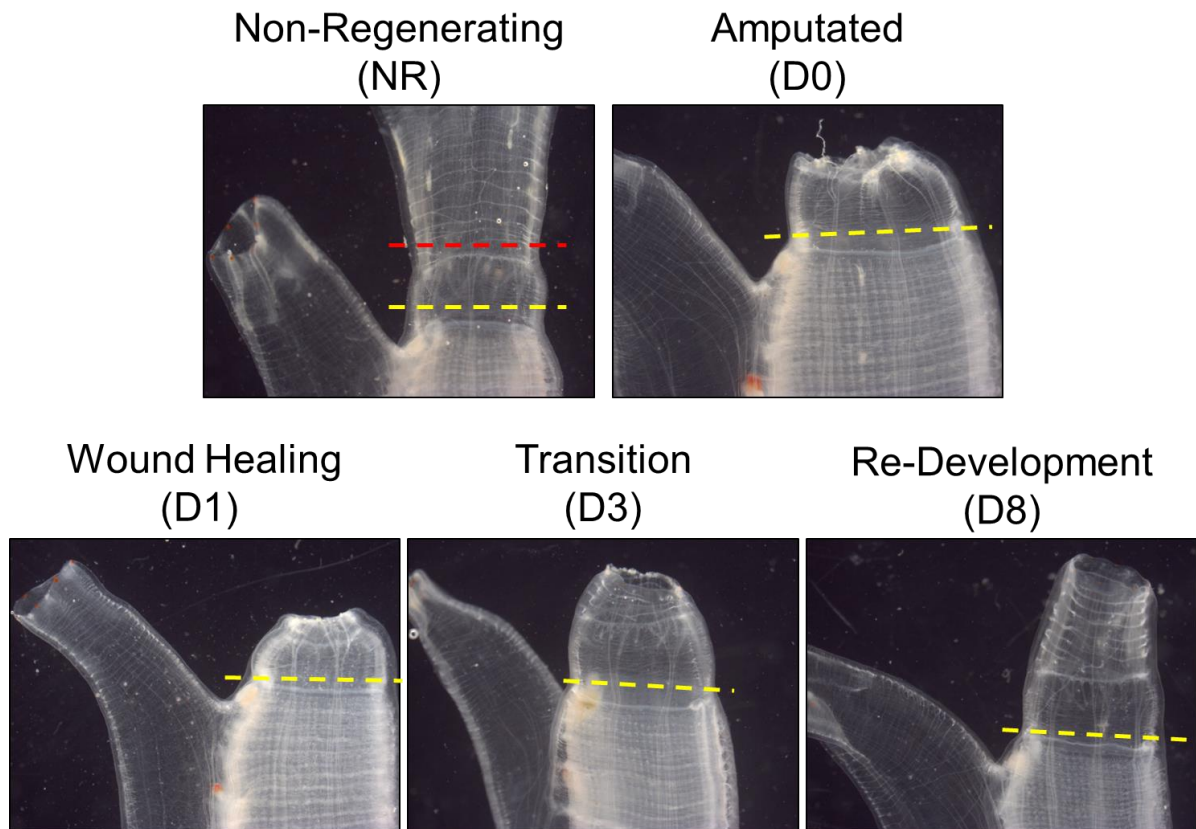
Figure 4. Stages of Oral Siphon Regeneration. (Top) The two reference stages used to quantify relative expression levels at subsequent stages. Left image shows an unamputated/non-regenerating (NR) adult oral siphon (OS) of C. robusta; the right image is immediately post-amputation. (Bottom) Three time points (D1, D3 and D8) selected to represent three stages of appendage regeneration (wound healing, transition and redevelopment, respectively). The red dashed line indicates the original amputation plane, and the yellow dashed lines indicate the proximal limit of tissue collected for expression profiling. Scale bars: 5 mm.

RNAseq) of miRNAs and mRNAs, then comparing relative expression levels between distinct stages of regeneration. I identified the largest changes in gene expression during OS regeneration and conducted a systematic characterization of functional categories of all genes as well as those predicted to be targeted by specific miRNAs. This study provides a resource that will facilitate future investigation into the genetic requirements of appendage regeneration in

chordates. To make our results comparable with those of a previous microarray study (Hamada et al., 2015) I also sequenced RNA from non-regenerating (NR) OSs (Fig 4) and identified several of the same genes they identified as the most significantly DE at 3 days post-amputation (D3).

III.A. Optimizing RNA Isolation from the OS

Standard RNA extraction methods (e.g. fresh tissue homogenization in Trizol at RT) proved ineffective at obtaining non-degraded RNA from adult OS tissue samples. I hypothesized the difficulty of extraction could be due to any of the following three reasons: 1) high polysaccharide content in the extracellular matrix and extracorporeal cellulose-based covering (the tunic) of adult ascidians, 2) high concentration of RNase enzymes present in the OS tissue, or 3) low RNA concentration produced by the cells residing in the OS.

To address the latter possibility, that the OS contained low concentrations of endogenous RNA, multiple siphons were pooled into single samples before homogenization in a 5ml glass dounce homogenizer. However, this did not improve the quantity or quality of the resulting RNA determined by NanoDrop spectrophotometry and formaldehyde-agarose gel electrophoresis, respectively. Tunics were manually removed from adult animals prior to amputation in an attempt to reduce the amount of polysaccharides and undesirable material present in the homogenate; however, this also failed to improve yield or quality of the resulting RNA. In

future preparations, tunics were always removed, because they proved largely insoluble in all lysis buffers, and thus removal facilitated homogenization of the underlying tissue.

Finally, to address the possibility that RNA was being degraded during the homogenization step, likely due to high concentrations of RNase present in the OS tissue, I began to perform RNA extractions on tissues snap-frozen in liquid nitrogen immediately after amputation. The frozen tissues were then transferred to RNAlater-ICE, which penetrates the tissue and prevents RNA degradation while the sample thaws from -192°C (liquid nitrogen) to -20°C (dry ice). Tissues were then kept submerged in RNAlater-ICE (Life Technologies) at -20°C for at least 24 hours until they were homogenized in either Trizol or an SDS based lysis buffer at RT using standard protocols. This method yielded total RNA in high quantities with almost no detectable degradation. I obtained RNA Integrity Number (RIN) scores of approximately 9.8 ± 0.2 (with 10 being completely non-degraded RNA) for all twelve samples used for mRNA library construction, as measured by an Agilent BioAnalyzer 2100 system.

III.B. Comprehensive Expression Profiling Using RNA-Seq

As a preliminary study, high throughput RNAseq was used to estimate relative abundance of mRNAs and miRNAs in non-regenerating (NR) OSs of 6 month-old *C. robusta* adults. In this initial validation of our approach, mRNA samples were collected from NR OSs and used to estimate efficiency
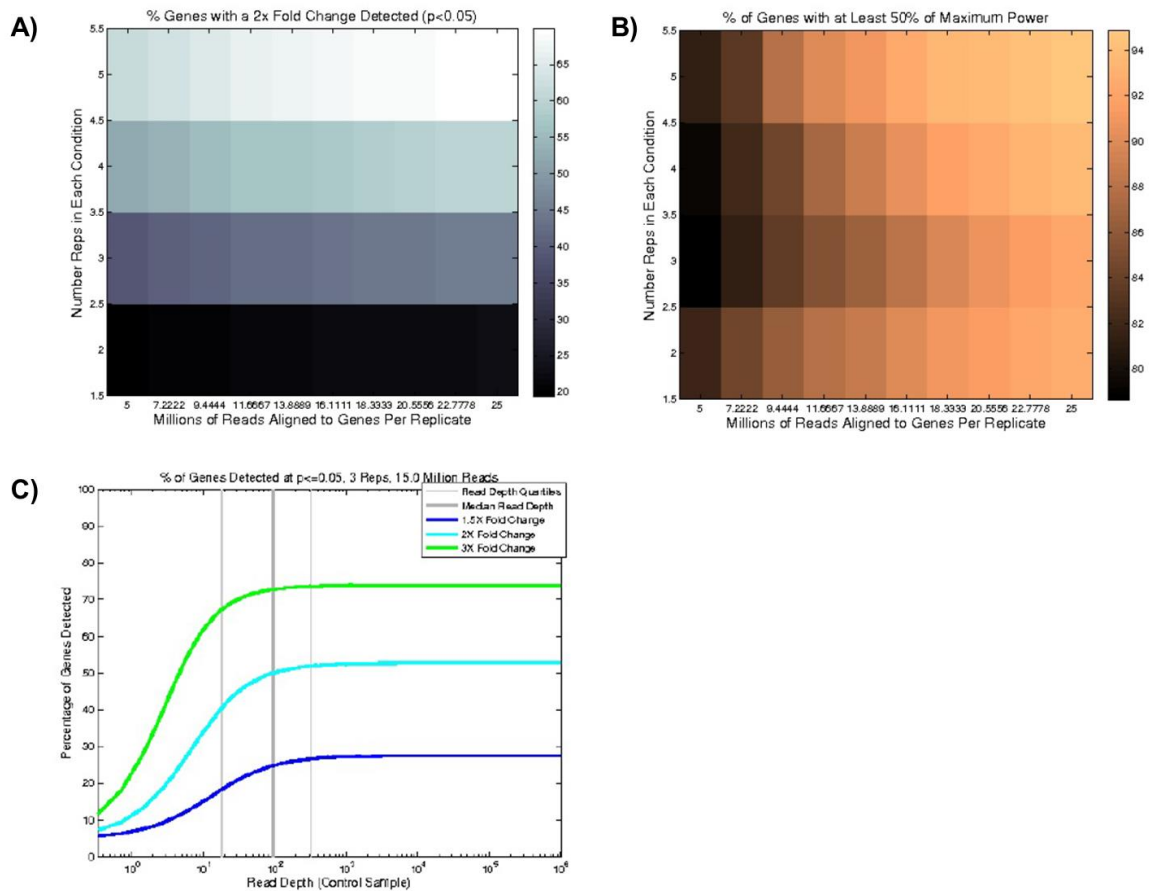
Figure 5. Pilot Study and Power Analysis of Non-Regenerating Oral Siphons. (A) Power of different experimental designs. Power is measured by the percentage of transcripts having a true 2X fold change detected at $p \leq 0.05$ using a t-test. (B) Measurement bias of different experimental designs. Maximum power is defined as the percentage of transcripts that could be detected if continuous sampling was performed. Then, measurement bias is defined as the percentage of transcripts sampled with at least 50% of the maximum power. (C) Expected true positive rates for our chosen experimental design. Curves indicate percent of differentially expressed transcripts expected to be detected at different levels of fold-change.

of read alignment and power to detect DE genes based on sequencing depth

and number of replicates. In this preliminary analysis, I successfully aligned

an average of 92.6% (94.8% across all stages) of sequencing reads to the *C.*

robusta genome with roughly 63.6% (58.4% across all stages) of reads

aligning to unique genomic locations (Appendix 1). Next, I estimated the

power of our chosen experimental design to accurately quantify differential

expression using the Scotty web tool (Busby et al., 2013). Given the sequencing depth and variation within the NR OS samples, I could expect to recover nearly half of the genes that are DE greater than 2-fold at any stage as significantly DE (FDR ≤ 0.05) using our experimental design (Fig. 5).

III.B.1. Differential expression of mRNA and microRNA

For collection of regenerating tissue samples, animals were amputated distal to the buccal tentacle band (Chiba et al., 2004) (Fig. 4). Either immediately following amputation (Day 0; D0) or one, three or eight days following amputation (D1, D3, and D8) tissue was collected by making a second cut proximal to the first, but distal to the peripharyngeal (transverse) muscle band (Fig. 4, yellow dashed lines). These time points were chosen to represent three stages of regeneration observed in vertebrates: wound healing, transition and redevelopment. Previous reports of differential expression had used NR OSs for comparison (Hamada et al., 2015). It was expected that comparisons of subsequent stages to either D0 or NR OSs would generate different categories as being enriched, and that by using both, a fuller picture would be generated. Three biological replicate cDNA libraries of each type (miRNA and mRNA) were prepared from the D0, D1, D3 and D8 tissue samples. In total, 12,700 of the 17,745 *C. robusta* mRNA transcript models were detected in the mRNA library sequence reads using a threshold of ≥ 5 RPKM in 3 or more samples.

Table 3. Number of Differentially Expressed Transcripts Relative to D0.

Sample Type	Method	LRT	D1 (+/-)	D3 (+/-)	D8 (+/-)
microRNA	EdgeR	15	4/11	4/11	6/9
	DESeq2	23	8/15	7/16	8/15
	Concurrence	14	4/10	4/10	5/9
mRNA	EdgeR	337	178/159	204/133	186/151
	DESeq2	472	244/228	254/218	252/220
	Concurrence	248	132/116	150/98	138/110

Note: Transcripts included in pairwise comparisons (D1, D3 or D8 vs. D0) were selected using likelihood ratio tests (LRT) (FDR ≤ 0.05) by either EdgeR, DESeq2 or the concurrence of both programs. The total number of differentially expressed transcripts across all comparisons determined by LRT is indicated as well as the number of transcripts up/down (+/-) regulated for each pairwise comparison.

Analysis was performed using two programs in parallel, EdgeR (Robinson et al., 2010), and DESeq2 (Love et al., 2014a). Only those transcripts identified as DE by both programs were used in order to reduce the likelihood of false positives, as has been described previously (Robles et al., 2012). The EdgeR and DESeq2 programs identified 337 and 472 of the mRNA transcript models, respectively, to be DE [false discovery rate (FDR) ≤ 0.05] on at least one day of regeneration (i.e., D1, D3 or D8) when compared to D0. Of the DE genes on these two lists, 248 overlapped (Table S2 of Spina et al., 2017). There were roughly an equivalent number of mRNAs up or down-regulated (Table 3). I assessed the expression of 15 DE mRNA transcripts using quantitative real-time

PCR (qRTPCR), with particular attention to transcripts linked to morphogenetic processes and signaling pathways (Fig. 6A). Of these, 9 were validated using qRTPCR in at least one stage during regeneration (Fig. 6A). For example, transcripts for the tumor necrosis factor receptor (TNFr) and an auxiliary protein (TNFr-associated) were found to be significantly ($p \leq 0.05$) downregulated by both RNAseq and qRTPCR at all stages post-amputation (Fig. 6A). I also confirmed that the expression of two potential activators of transforming growth factor-ß (TGF-ß) signaling were significantly upregulated during regeneration (Fig. 6A). These two pathways have previously been implicated in regulation of programmed cell death and proliferation during regeneration (Gilbert et al., 2013; Godwin et al., 2013; Ho and Whitman, 2008; Lévesque et al., 2007; Rao et al., 2009; Stoick-Cooper et al., 2007; Wu et al., 2013).

The miRDeep2 program (Friedländer et al., 2012) was used to align and quantify miRNA reads. Most of the miRNAs I detected during OS regeneration have been described previously (Hendrix et al., 2010; Keshavan et al., 2010; Missal et al., 2005; Norden-Krichmar et al., 2007; Shi et al., 2009; Terai et al., 2012). However, miRDeep2 also predicted 52 previously undescribed (novel) miRNAs with an estimated probability that a reported novel miRNA is genuine equal to $95 \pm 3\%$ (Table S3 of Spina et al., 2017). The most highly expressed of these novel miRNAs, *1_2011*, was found to have an identical seed sequence to *hsa-miR-4709-5p* and was detected at over 50-fold greater number of reads than the second
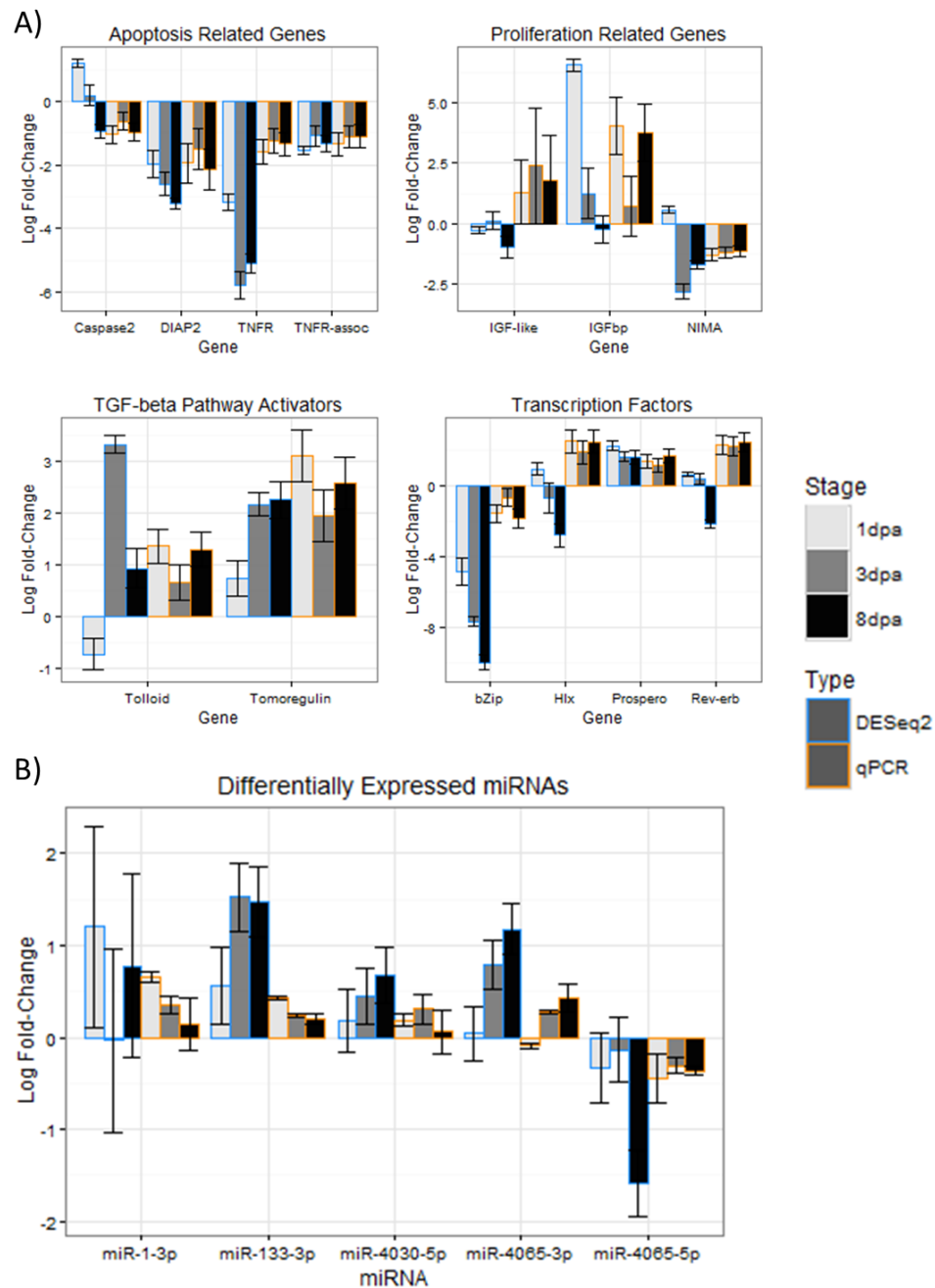
Figure 6. Experimental validation of differential expression. The mean $\log_2$ fold change of transcript expression levels relative to D0 estimated by RNAseq (DESeq2) and qRT-PCR. Three biological replicates comprising three technical replicates each were used to calculate qRT-PCR statistics; error bars indicate s.e.m. for RNAseq and 95% confidence intervals for qRT-PCR. (A) Differentially expressed (DE) mRNAs significant in both RNAseq and qRT-PCR experiments arranged into preselected groups. Ensembl transcript identifiers matching each transcript name are listed in Table S8. (B) DE miRNAs significant in both RNAseq and qRT-PCR data.

23

most highly expressed novel miRNA. Another novel miRNA, *12_9033*,

was found to be strongly and significantly upregulated during

regeneration. Overall, out of the 550 known miRNAs in miRBase

(Griffiths-Jones, 2004; Kozomara and Griffiths-Jones, 2014) plus the

novel miRNAs predicted by miRDeep2, I detected 279 miRNAs in the

miRNA library reads at a threshold of $\geq$ 1 CPM in 3 or more samples.

Comparisons were made between miRNA transcripts in the newly

amputated siphon (D0) to each of the three days of regeneration (D1, D3

and D8). Of the 279 miRNAs expressed, 15 and 23 were found to be DE

on at least one day of regeneration by EdgeR and DESeq2, respectively.

Of the DE miRNAs identified by EdgeR, 14 were also identified by

DESeq2 (Table 3 and Appendix 3). In contrast to the mRNAs, there were

approximately twice as many miRNAs significantly downregulated

versus up, suggesting an active role for miRNAs in adult OS homeostasis.

The total number of DE transcripts for each day of regeneration is shown

in Table 3.

Several DE miRNAs were also selected for validation based on their

large estimated fold-change, significance of relative change, or previous

reports indicating roles for these miRNAs in morphogenetic and

regenerative processes (Fig. 6B). In regenerating OSs *miR-9* is highly

upregulated at all stages of regeneration analyzed, having no RNAseq

reads and being nearly undetectable by qRTPCR at D0. Additionally, the

bicistronic *miR-1/133* (Kusakabe et al., 2013), which has been implicated

in muscle development and regeneration (Mitchelson and Qin, 2015; Yin et al., 2008) was also upregulated during OS regeneration. In summary, the relative expression changes estimated by RNAseq for 9/15 mRNA transcripts (60%) were validated using qRTPCR in at least one stage during regeneration. Likewise, I were able to validate that 10/17 miRNAs (58.8%) were significantly changed during at least one stage.

III.B.2. Comparing between Stages of Regeneration

In addition to identifying DE transcripts following amputation, enrichment for functional categories of genes was performed using classifications curated by the Gene Ontology (GO) Consortium (Ashburner et al., 2000) and the Kyoto Encyclopedia of Genes and Genomes (KEGG) Pathway Database (Kanehisa and Goto, 2000) (Table S8 of Spina et al., 2017). Enrichment of functional categories based on the mean significance ($-\log2$ FDR) of genes within each category was performed by comparing the three days of regeneration (D1, D3 and D8) with either D0 (Fig. 7) or NR OSs (Fig. 8). The complete list of z-scores for all categories relative to either reference stage is listed in Table S9 of Spina et al., (2017).

Several GO Biological Process (BP) categories showed a pattern of enrichment across all stages, including 'negative regulation of peptidase activity', 'xenobiotic metabolic processes', 'protein folding', 'cellular calcium ion homeostasis' and 'multicellular organismal development'
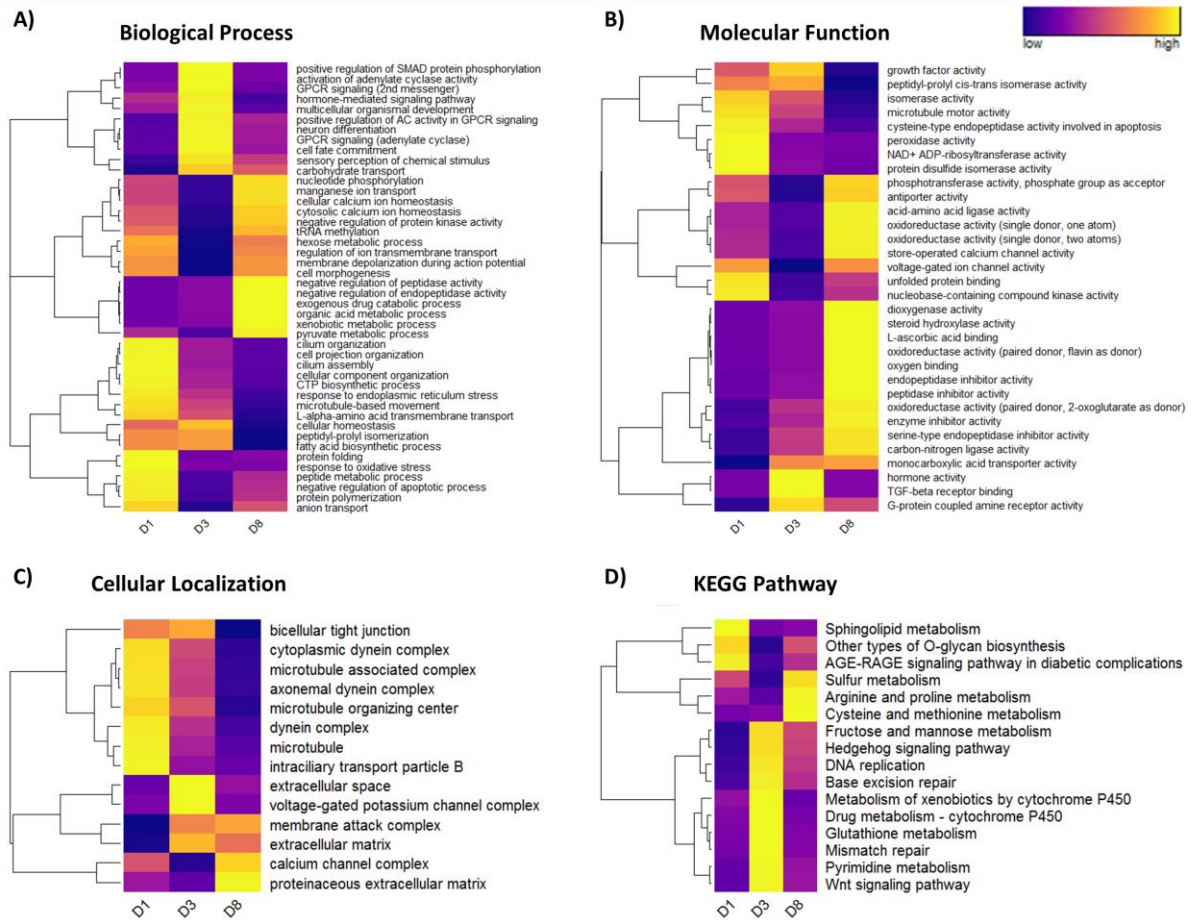
Figure 7. Standardized Z-scores of Enriched (z≥1.96) Functional Categories Relative to D0. Z-scores, plotted as heatmaps, were calculated relative to D0 then standardized across post-amputation stages D1, D3 or D8. Dendrograms to the left of each heatmap indicate the results of hierarchical clustering of the indicated GO categories (A-C) or KEGG pathways (D).

(Fig. 7A). Similarly enriched GO Molecular Function (MF) categories included 'peptidase inhibitor', 'heme binding', 'unfolded protein binding' and 'growth factor activity' (Fig. 7B). For the most part, categories modified across the 8 days of regeneration studied are consistent with a pattern of activated cellular growth and metabolism.

Other categories were enriched during specific stages of regeneration. As expected, categories enriched early in regeneration (D1
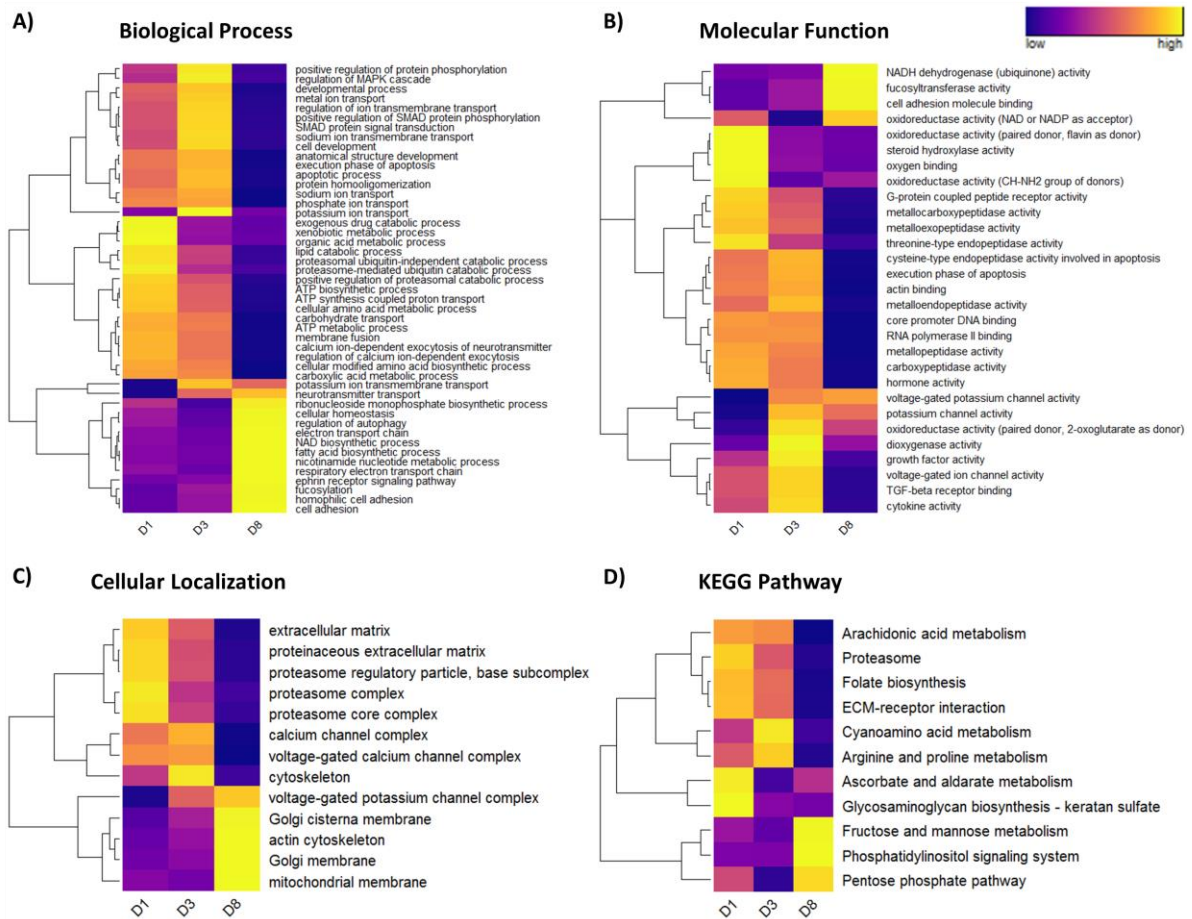
Figure 8. Z-scores of Enriched (Z ≥ 1.96) Functional Categories Relative to Non-Regenerating Oral Siphons. Z-scores plotted here as heatmaps were calculated relative to non-regenerating (NR) oral siphon samples then standardized relative to the mean & standard deviation across stages. Dendrograms to the left of each heatmap indicate the results of hierarchical clustering the categories. Stages are listed below each column of the heatmaps while categories are listed to the right. (A) GO Biological Process. (B) GO Molecular Function. (C) GO Cellular Localization. (D) KEGG Pathways.

and D3) included those related to wound healing, stress response, activation of morphogenetic processes and signaling. For example, the KEGG pathway 'AGE-RAGE signaling in diabetic complications' (which includes upregulated immune/stress-response genes like JAK1, STAT5A and Jun) was enriched only at D1 (Fig. 7D). GO categories enriched exclusively at D1 include 'response to endoplasmic reticulum stress',

'cilium organization', 'protein polymerization', 'steroid biosynthetic processes' and 'cysteine type endopeptidase activity involved in apoptosis'. Other categories enriched at both D1 and D3 include 'microtubule-based movement and motor activity', 'hormone-mediated signaling', 'fatty acid biosynthesis', 'cellular homeostasis' and 'bicellular tight junction'.

Likewise, a number of categories with the potential to directly regulate morphogenetic processes during regeneration were enriched exclusively at D3. KEGG pathways enriched at this stage included 'glutathione metabolism', 'DNA replication' and 'Wnt signaling' (Fig. 7D). Corresponding GO categories enriched at this stage included 'steroid hormone-mediated signaling', 'steroid hormone receptor activity', 'G-protein-coupled receptor activity', 'metalloendopeptidase activity' and 'voltage-gated potassium channel complex'.

Finally, categories enriched in later stages are expected to be involved in a return to homeostasis of the regenerating tissue, but could also represent downstream effects of changes observed at earlier stages and thus might not be exclusively enriched at late stage expression. Categories enriched only at D8 appeared to be less associated with signaling pathways but instead more related to tissue growth, such as 'glucose import', 'negative regulation of protein kinase activity' and 'amino acid transmembrane transporter activity'.

III.B.3. Requirement of TGF-β Signaling

The increased expression of TGFß activators observed post-amputation suggests a role for this signaling pathway in OS regeneration (Fig. 6). This was further supported by enrichment of functional categories related to TGFß signaling at 3 days post-amputation (D) (Fig. 7A, B). It has been previously reported that TGFß signaling is required for multiple events during regeneration of *Axolotl* limbs, *Xenopus* tadpole tails and *Eublepharis* tails (Gilbert et al., 2013; Ho and Whitman, 2008; Lévesque et al., 2007). To investigate whether TGFß is also required during OS regeneration, I treated amputated *C. robusta* juveniles with 10 µM SB431542, a potent and specific inhibitor of activin receptor-like kinase receptors that mediate TGFß signal transduction (Mita and Fujiwara, 2007).

Soaking *C. robusta* in SB431542 for 4 days following amputation completely blocked regeneration (Fig. 9). Whereas 100% of control-treated animals regenerated OPOs by D8, none of the SB431542-treated animals showed any visible signs of regeneration (Table 4). To further refine the temporal requirement for TGF-ß signaling, I treated separate cohorts of animals with SB431542

Table 4. Number of Animals with Regenerated OPOs after SB431542 Treatment

Cohort	Duration	4dpa	8dpa
DMSO	4 days	56/67	61/67
0-4	4 days	0/28	0/20
0-1	24 hrs	0/11	0/11
1-2	24 hrs	2/13	8/13
2-3	24 hrs	0/11	3/11
3-4	24 hrs	4/9	5/9
0-2	48 hrs	0/27	0/20
1-3	48 hrs	0/28	0/20
2-4	48 hrs	0/28	0/20

Note: Cohort names correspond to conditions illustrated in Fig. 9A
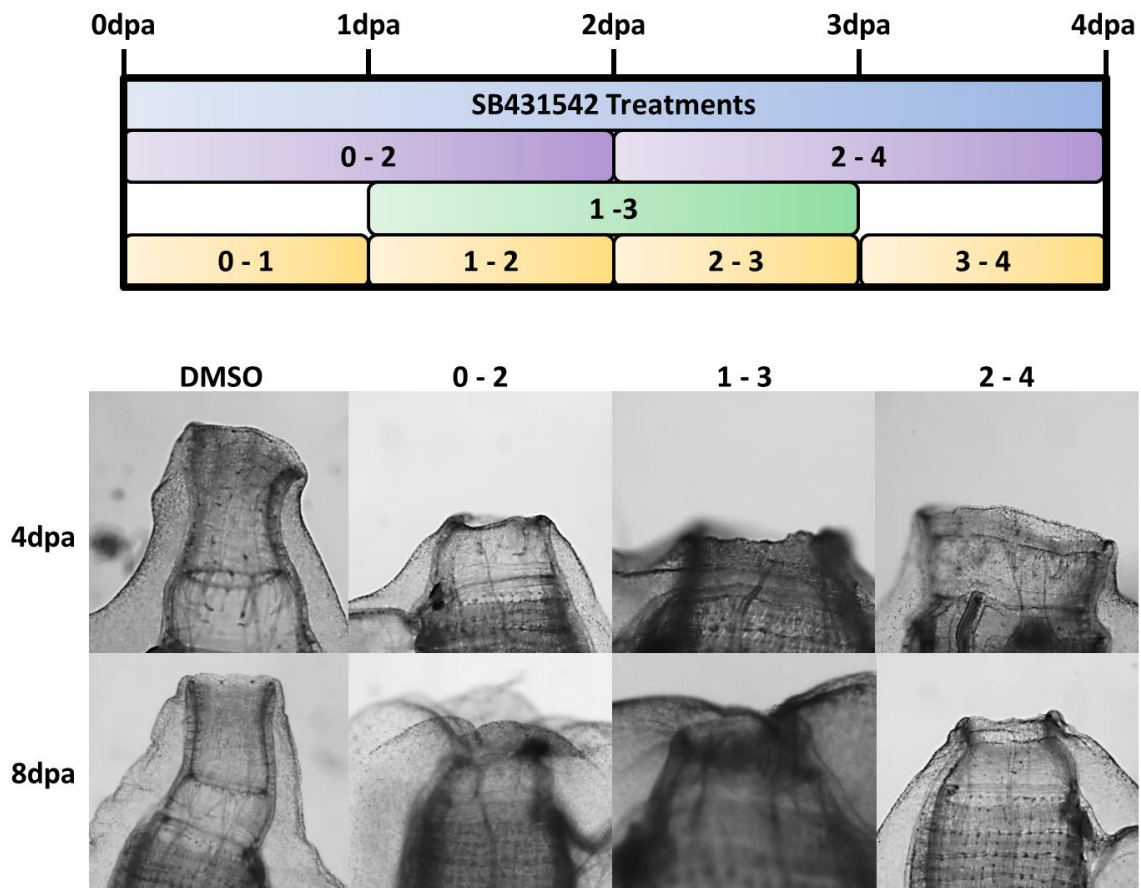
Figure 9. SB431542 treatment of *C. robusta* juveniles. Approximately 1-month-old animals were treated with 10 µM SB431542 for the durations illustrated in the diagram (top). Images of representative animals from the 48 h treatment cohorts show inhibited OS regeneration (bottom). DMSO was used as the vehicle control. See also Table 4.

over 24 h periods for each of the 4 days following amputation (Fig. 9).

Surprisingly, only the cohort treated over the first 24 h following

amputation failed to regenerate completely, whereas the other three

cohorts showed partial OPO regeneration (Table 4). The temporal

requirement was further studied using three cohorts of animals treated

with SB431542 for 48 h periods starting either (1) immediately after

amputation, (2) 24 h after amputation or (3) 48 h after amputation (Fig.

9). These 48 h treatments completely blocked regeneration in all cases

(Fig. 9), indicating that TGFß signaling is required on at least two separate occasions during OS regeneration (once during a short window in the first 24 h, then again during a second >24 h window that includes 3 D).

III.B.4. Molecular Signatures of Evolutionary Conservation

Appendage regeneration is thought to occur in three morphologically distinct stages: wound healing, transition and redevelopment (Knapp et al., 2013). The wound healing stage is primarily defined by a localized immune response, closure of the epithelium and initiation of blastema formation (Murawala et al., 2012). I observed several transcriptional changes indicating conserved features of wound healing during OS regeneration. GO categories supporting this hypothesis that are enriched at D1 include 'response to ER stress', 'response to oxidative stress', 'protein folding', 'unfolded protein binding', 'cysteine-type endopeptidase activity involved in apoptosis' and the KEGG pathway 'AGE-RAGE signaling pathway in diabetic complications' (Fig. 7).

Following healing, a transition occurs in which the remaining appendage begins to redevelop the lost tissue. During this transition phase, positional identity is regained and signaling to activate progenitor cells, which are required to initiate growth, occurs. Insulin growth factor (IGF) signaling was first implicated in limb regeneration in newts over three decades ago (Vethamany-Globus, 1987). More recently, it was

discovered that IGF secreted from wounded zebrafish epithelia stimulates underlying mesenchymal blastema cells to proliferate (Chablais and Jazwinska, 2010). Further, it has been hypothesized that a Warburg effect (Vander Heiden et al., 2009) can be promoted in regenerating vertebrate tissues to favor structural biosynthesis over generation of ATP (Love et al., 2014b). I observed high levels of IGF and IGF binding protein (IGFbp) transcript levels throughout regeneration (Fig. 6). IGF binding proteins have been reported to act as carriers for IGF to promote increased persistence of IGF in circulation (Hwa et al., 1999). Further investigation into the role of IGF signaling during OS regeneration could help determine whether the effects of this signaling pathway on cell proliferation and energy metabolism in different models of vertebrate regeneration are likely to be derived from a common evolutionary origin.

The transverse vessels of the branchial sac in *C. robusta* are thought to contain progenitor cells required for OS regeneration that are activated to proliferate and migrate into the OS after amputation (Jeffery, 2015b). Although the extent to which these branchial sac stem cells contribute to various tissues has not yet been investigated, it is suggested that they have the potential to differentiate into multiple lineages due to high expression of pluripotent cell marker genes such as Piwi and Alkaline phosphatase (Juliano et al., 2011; O'Connor et al., 2008; Štefková et al., 2015). Piwi-positive stem cells in colonial tunicates

are essential for whole-body regeneration (Brown et al., 2009) and also originate from a vascular niche (Rinkevich et al., 2010). Cells of the branchial sac divide following amputation (Jeffery, 2015b); however, EdU and phospho-histone H2 labeling of regenerating OSs showed no detectable increase in the number of dividing cells per unit area until ~4 D (Auger et al., 2010). I observed transcriptional changes supporting the proposed timing of proliferation, such as the enrichment at D3 of the KEGG pathways 'DNA replication' and 'Wnt signaling' along with the GO categories 'TGFß receptor binding', 'cell fate commitment' and 'growth factor activity' (Fig. 7).

Our identification of the requirement for TGFß signaling at 3 D, as indicated by the lack of subsequent tissue regrowth and OPO differentiation following SB431542 treatment, as opposed to any potential disruption of patterning or the null hypothesis of no effect, further supports the hypothesis that a progenitor population is receiving inductive signals, putatively TGFß itself, at this stage in order to stimulate proliferation and regeneration of lost tissue. Further studies comparing localization of TGFß pathway members and effects on proliferation after SB431542 treatment during OS regeneration could identify the mechanism by which this pathway regulates regenerative regrowth and differentiation.

Once progenitor cells have been specified and positional identity within the regenerating tissue is established, the latter stages of regeneration are thought to proceed in a similar manner to how the original appendage/tissues were formed during development. This process involves extensive remodeling of the extracellular matrix (ECM) to regulate cellular responses such as apoptosis, proliferation, migration and differentiation (Calve et al., 2010; Lu et al., 2011). ECM remodeling is regulated via activation of specific enzymes such as Serpins (Simone et al., 2014) and TIMPs (Arpino et al., 2015), which inhibit peptidases that degrade structural ECM proteins. I observed strong enrichment of the GO categories 'peptidase inhibitor' and 'negative regulation of peptidase activity' at later stages of regeneration, particularly at D8 (Fig. 7). This supports the hypothesis that OS regeneration involves substantial ECM remodeling at early and mid-stages, which is actively attenuated by expression of peptidase inhibitors such as serpins and TIMPs at later stages.

A microarray-based study of gene expression during OS regeneration was recently published (Hamada et al., 2015). This study reported the 30 genes with the largest changes relative to NR OS at 3, 6 and 9 D. I compared the list of genes reported as DE at day 3 of regeneration with an analogous list derived in this study (Table S4 of Spina et al., 2017). When converting from the gene identifiers used on the microarray, I were

able to identify Ensembl gene models for 26 out of the 30 microarray probe sets listed. Of these Ensembl transcript models, 18/26 transcripts were expressed above the threshold of 5 RPKM in at least three or more samples, but only 6 of these 18 were identified as DE (FDR ≤ 0.05) by DESeq2, 5 of which were confirmed by EdgeR, notably including Notch and EphA4.

III.C. A Network of miRNA Target Interactions

I derived a non-biased correlation-based network to infer a comprehensive set of miRNA-target interactions over the course of 8 days of OS regeneration. Several transcriptome-wide miRNA profiling studies have been performed during limb or appendage regeneration (Gearhart et al., 2015; Holman et al., 2012; Thatcher et al., 2008), although not in parallel with mRNA transcriptome analysis. miRNAs primarily exert their effects on gene products through degradation or translational repression of target RNAs (Carthew and Sontheimer, 2009). In the absence of proteomic data, our analysis is limited to those cases in which miRNA-mRNA interactions result in degradation of the target mRNA. If I optimistically assume that all miRNAs result in degradation of their target transcript(s), then strength of miRNA-mRNA interactions can be estimated by identifying miRNA-target pairs that display inverse (negative) correlations between different stages of a process.
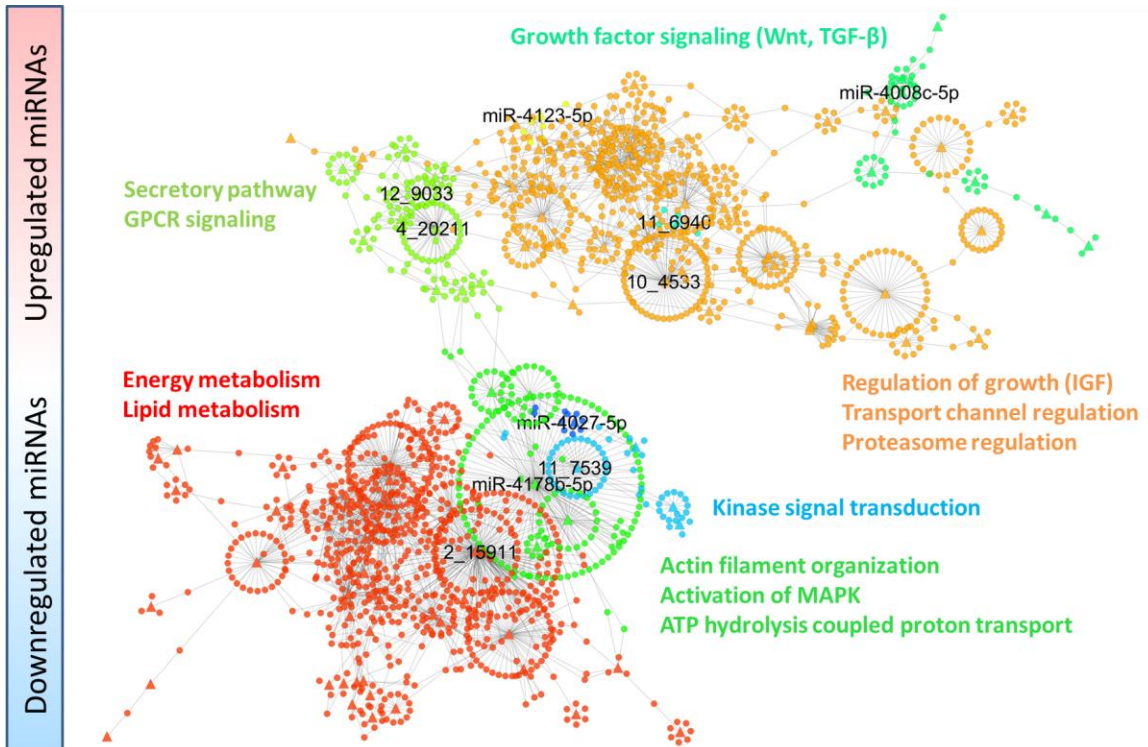
Figure 10. miRNA-mRNA correlation network. miRNAs and mRNAs are represented by triangles and circles, respectively. Transcripts are joined by a line when both ρ≤−0.9 and a binding interaction was predicted by TargetScanS. ModuLand clusters are shown in different colors and the miRNA ID that defines each cluster is indicated (black text). Summary interpretations of enriched GO categories and KEGG pathways in each cluster are indicated in matching colors adjacent to the respective cluster. The full set of correlations, assignment of nodes to clusters and functional enrichments for clusters are listed in Table S12 of Spina et al., 2017.

A preliminary step in this analysis is prediction of complementary sequence pairing between the full set of miRNAs (including novel miRNAs identified in this study) and the 3′-UTRs of potential target transcripts. I accomplished this using TargetScanS (Agarwal et al., 2015; Lewis et al., 2005), which was first employed to detect conserved binding sites between *C. robusta* and *C. savignyi*, before identifying additional non-conserved sites in non-orthologous genes. Our complete set of target predictions for *C. robusta* (conserved and non-conserved) contained ~521,000 pairwise interactions and

is available for download (https://labs.mcdb.ucsb.edu/smith/william). Notably, within the conserved set of predictions between *C. robusta* and *C. savignyi* I identified the same 824 targets for miR-124 as reported by another study (Chen et al., 2011), which identified miRNA seed pairing as a strong predictor of target downregulation in *Ciona*. Thus, I expect a large proportion of the predictions to be relevant in vivo. Further support for the relevance of these predictions was found by identifying a large proportion of the predicted miRNA-target pairs that are conserved with other species and have been validated experimentally (either by expression profiling, reporter assay or western blot) by comparing with information listed in miRTarBase (Chou et al., 2016) (data not shown).

The average log2 fold-change estimated by DESeq2 and EdgeR at all stages (D0 versus D1, D3 or D8) was used to calculate Pearson correlation coefficients (ρ) for all predicted miRNA-target pairs. Subsequent analysis was limited to miRNAs with observed changes$\geq$|1 log2-fold| at any stage and $\rho\leq-0.9$ with their predicted targets. The resulting directed network contained 2033 nodes (129 miRNA, 1904 mRNA) and 2854 edges, with an average of 2.808 neighbors per node (Table S10 of Spina et al., 2017). Evolution of biological networks is assumed to have proceeded by preferential attachment of new nodes to an existing core network, resulting in a 'scale-free' topology that can be modeled using a power law function (Albert, 2005; Barabási and Oltvai, 2004; Wolf et al., 2002). Biological

networks tend to grow through preferential attachment to hub nodes (heavily skewed distribution), versus random attachment to any node in the network (normal distribution), which results in a topology that resembles social networks or the distribution of people in large cities surrounded by many small towns. The in-degree distribution of edges/nodes in our network was fit to a power law curve with the equation $y=2919.4x-3.362$ ($\rho=0.983$, $R^2=0.917$), suggesting the topology of our predicted network indeed resembles that of a true biological network. Plotting these interactions shows a dense cluster of downregulated miRNAs associated with a dense cluster of upregulated mRNAs, joined by a few sparse connections (Fig. 10).

To assign putative functions to miRNAs within the correlation network, I implemented a clustering algorithm on all the nodes and then examined whether the list of targets in each cluster were enriched for particular GO categories and KEGG pathways. Non-overlapping clusters of miRNAs and targets were identified by analyzing the correlation network using the LinkLand algorithm (Kovács et al., 2010) provided by the ModuLand plug-in (Szalay-Bekő et al., 2012) for Cytoscape (Smoot et al., 2011). Briefly, each node is assigned a set of influence scores that relate it to all other nodes in the network based on their relative position and connections. Next, clusters are determined by identifying local maxima (which indicate the centers) and local minima (which define the boundaries) of influence scores throughout the network. The miRNAs and targets assigned to each cluster are listed in Table S11 of Spina et al., 2017. All of the targets within each resulting

cluster were grouped and then the significance of overlap between each

cluster and GO/KEGG functional categories was assessed using a

hypergeometric test for enrichment, which describes the probability of a

predefined number of successes (transcripts in each cluster) out of the

number of draws from a pool of possibilities (transcripts in a given functional

category) (Table S12 of Spina et al., 2017). Interpretations summarizing the

significantly enriched functional categories are shown alongside their

respective color-coded miRNA-target clusters in Fig. 10.

III.C.1. Assigning Stages and Functions to Network Clusters

I observed significant overlap between transcripts in certain functional

categories and particular miRNA-target clusters. For example, categories

related to 'immune response', 'stress responses' and 'apoptosis' were

enriched at D1 relative to D0. These categories also significantly overlapped

with miRNA-target clusters miR-4178b-5p and 4_20211. Further,

attenuation of apoptosis and induction of morphogenetic growth factor

signaling are crucial for the transition from wound healing to the activation

of redevelopment. Several miRNA clusters were found to target mRNAs

annotated in functional categories related to Wnt, TGFß and MAPK

signaling, as well as regulation of apoptosis and regulation of cell cycle

including miR-4008c-5p, miR-4123-5p, miR-4178b-5p, 2_15911, 4_20211 and

11_7539. Finally, during the redevelopment stage I observed strong

enrichment of ECM peptidase inhibitors (Fig. 7), which significantly

overlapped with the miRNA-target clusters miR-4008c-5p, 10_4533 and 11_6940.

During all stages of regeneration I observed increased levels of IGF and IGFbp transcripts (Fig. 2A). The GO MF categories 'insulin receptor binding' and 'insulin-like growth factor binding' significantly overlapped with the miRNA-target cluster 10_4533 (Table S12 of Spina et al., 2017), which is supported by significant overlap between the group of mRNAs targeted by this cluster and the GO BP categories 'regulation of cell fate specification', 'regulation of cell growth' and 'regulation of mitotic cell cycle'. This miRNA-target cluster might also be involved in regulating multiple unrelated processes at specific stages of regeneration. First, this cluster significantly overlaps with the categories 'unfolded protein binding' and 'regulation of apoptotic processes', which are enriched at the D1 stage (Fig. 7). Second, as mentioned previously, the miRNA-target cluster 10_4533 significantly overlaps with the GO MF category 'endopeptidase inhibitor activity', which is highly enriched at D8 (Fig. 7).

I observed miR-9, an ancient and well-conserved miRNA essential for normal function of developing and differentiated neurons (Coolen et al., 2013), to be specifically upregulated during regeneration. This miRNA has previously been identified as expressed during the gastrula and larval stages of *C. robusta* (Hendrix et al., 2010). In other species miR-9 has been shown to regulate differentiation via targeting of the Notch signaling pathway (Jing

et al., 2011; Kuang et al., 2012). The proliferative state of neural progenitors is governed by oscillations in the protein level of Hes1; high levels of miR-9 were shown to dampen oscillations of Hes1 leading to increased proliferation and differentiation (Bonev et al., 2012; Tan et al., 2012). Interestingly, I did not identify binding sites for miR-9 in any members of the Notch pathway or predicted downstream targets of Hes1 (data not shown). However, our 17 predicted targets for miR-9 do suggest a possible role in regulating differentiation and the proliferative state of neural progenitors through regulation of the cytoskeleton and cell cycle (Galderisi et al., 2003; McBeath et al., 2004). Functional categories significantly overlapping with miR-9 network cluster targets that are associated with cell cycle regulation are 'cell division', 'DNA replication initiation and DNA replication', which contain the miR-9 targets Nek7-like, SFI1-like and Myb-binding 1A. Categories significantly overlapping with miR-9 network clusters associated with cytoskeletal regulation are 'intermediate filament', 'cytoskeleton organization', 'microtubule-based movement', 'microtubule motor activity', 'kinesin complex' and 'microtubule binding', which include the miR-9 targets villin-1, Kinesin, sideroflexin-1-like, LIMK1-like, myosin X and LMNTD1.

III.C.2. Significance and Limitations of the Predicted Network

miRNA regulation is important in several well-studied examples of regeneration (Sen and Ghatak, 2015). miRNAs can either lead to direct degradation or translational repression of their target transcripts (Carthew and

Sontheimer, 2009). One obvious caveat of miRNA and mRNA transcriptional profiling is that translational repression cannot be detected. If a given miRNA is predicted to target a given transcript based on seed pairing and the expression levels of these two transcripts are inversely correlated, I infer the predicted interaction is specific and results in target degradation. Predicted target pairs that do not show an inverse correlation could still result in translational repression; however, the relevance and extent of this type of interaction was not considered in this study.

For 8 of the 22 clusters detected using ModuLand (Fig. 10), the most central nodes identified as representing each cluster were novel miRNAs identified in this study. This underscores the complementary nature of co-expression and differential expression analyses. Co-expression analysis was able to identify individual miRNA(s) with small relative fold changes as important during regeneration by virtue of the position of that miRNA within a correlation network. On the other hand, differential expression analysis did not identify many novel miRNAs to be important during regeneration but was able to identify miRNAs that had the largest fold changes at any stage.


IV. Cells Contributing to OS Regeneration

In order for a damaged or missing tissue to regenerate, the remaining tissue must integrate signals that indicate the location and severity of tissue injury then re-establish the positional identity of remaining cells and mobilize

progenitor cells to proliferate and differentiate in the appropriate manner. The signaling mechanisms regulating these processes, including TGF-ß, were investigated extensively in the previous chapters. However, the question of which cells are responding to these instructive cues remains unaddressed.

Progenitor cells often have the ability to differentiate into more than one mature cell type. The plasticity of regenerative progenitors ranges from the totipotent neoblasts observed in planaria, multipotent germ lineage-restricted progenitors in the salamander limb, and finally unipotential progenitors such as some hematopoietic precursors and liver hepatocytes. The outcome of whether any particular progenitor cell differentiates or undergoes a process of self-renewal (maintenance of the progenitor population) is determined by the surrounding cells and extracellular environment, collectively named the niche (Lane et al., 2014). Myself and others (Jeffery, 2015a) have attempted to identify the progenitors that contribute to OS regeneration as well as the location and composition of the niche which maintains this progenitor population.

IV.A. Evidence for Local and Migratory Sources of Progenitors

Four sets of experiments have demonstrated the existence of some ability for cells present in the OS prior to amputation to contribute to its regeneration. First, UV irradiation of only the OS (while shielding the remaining part of the animal) resulted in failed regeneration of the OS (Fig 11A, B; Auger et al., 2010). Radiation causes DNA damage and prevents

43
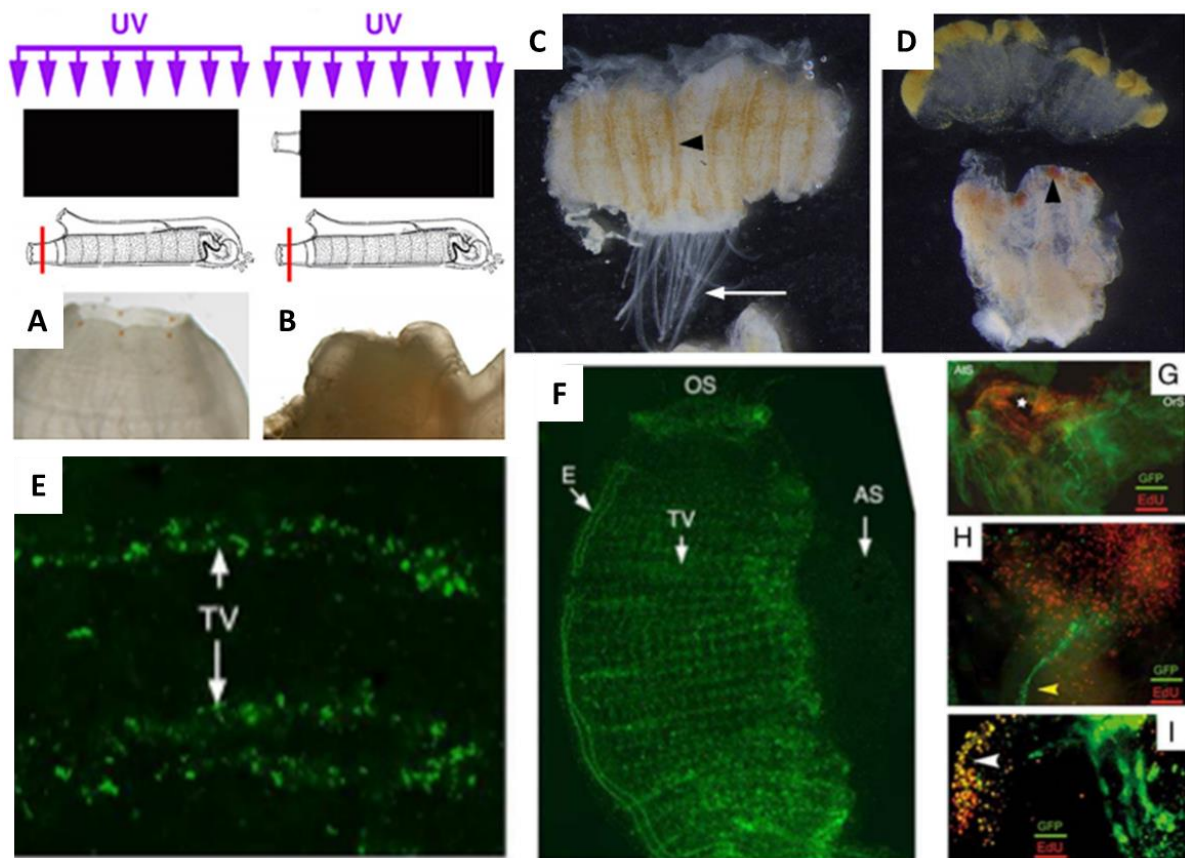
Figure 11. Cellular Proliferation and Differentiation during Regeneration in *Ciona*.
(A, B) OPO regeneration was blocked after global UV irradiation (A), but controls regenerated OPOs (B). (C) A mid-section explant after 6 days in culture with tunic removed that has been cut along its proximal–distal axis and opened to show columns of intense orange pigment cells (arrowhead) located in the ORB. The arrow indicates the tentacles, which mark the proximal side of this explant. (D) A mid-section explant after 9 days in culture with tunic removed (bottom) that was co-cultured with a tip explant (top) from the same animal. Arrowhead in panel D shows OPOs that appeared at the distal margin of the mid-section explant (bottom). No OPOs appeared at the proximal margins of the siphon tip (top) or mid-section explants (bottom) during the culture period. (A-D) reproduced with permission from (Auger et al., 2010). (E, F) EdU labeling of the basal regenerating parts of animals for 12 h (E) or 48 h (F) after OS amputation shows early labeling in the transverse vessels of the branchial sac and distal margin of the regenerating OS. (E-F) reproduced with permission from (Jeffery, 2015b). (G–I) Neuronal cells double-labeled with GFP and EdU in the E15 transgenic line at 4 dpa. (G) Low magnification showing a field of EdU-labeled proliferating cells surrounding the NC ablation zone (star). (H) A regrowing neurite (yellow arrowhead) surrounded by EdU-labeled cells. (I) A merged photograph showing a region of regenerating neuronal cells with overlapping EdU and GFP (yellow staining). OrS: oral siphon. AtS: atrial siphon. (G-H) reproduced with permission from (Dahlberg et al., 2009).

cells from replicating their genetic content during cell proliferation. Therefore, the partial irradiation experiments support the hypothesis that proliferation of resident oral siphon cells is somehow required for later events in regeneration. Second, explant cultures of amputated OS's demonstrated that pigment cells are capable of differentiating from a source of progenitors present in the OS prior to amputation (Auger et al., 2010)(Fig 11C, D). Third, whole animal EdU pulse-chase experiments during OS regeneration revealed broad staining in the branchial sac and a blastema region at the distal edge of the regenerating OS (Fig 11E, F; Jeffery, 2015b). Fourth, BrdU/EdU labeling of CNS regeneration suggests nerve regrowth is stimulated by proliferation of GFP labeled nerve cells present at the regenerating tip of the nerve (Fig 11G- I; Dahlberg et al., 2009). However, the exact source & lineage of the regenerated nerve cells remains unresolved, because even after long pulses of BrdU/Edu many of the regenerated nerve cells were still unlabeled, suggested they might originate from another lineage or simply not require proliferation to differentiate. It also remains unclear whether regenerating nerves in the OS incorporate migratory cells or are purely neural lineage in origin. Although the simplest explanation is that cells proliferating at nerve-tips are pre-existing nerve cells, however, it's possible that migratory progenitor cells home to the regenerating nerve tips where they then proliferate and trans-differentiate to form functional neurons.

In contrast to evidence for the requirement of pre-existing cells near the amputated region (specifically in pigment and nerve cell regeneration), there are also several lines of evidence to support the existence of migratory progenitor cells contributing to OS regeneration. It has been well established since the experiments of Mingazzini in 1891 that the posterior portion of a bisected adult *Ciona* can regenerate the lost anterior regions, such as the siphons and neural complex, while the anterior portion can never regenerate the lost posterior parts (Jeffery, 2015a). This suggests a source of pluripotent stem cells exists somewhere in the posterior part of the animal which might be capable of regenerating muscle, nerves, and vasculature while also coordinating (or being coordinated to produce) the correct patterning of the branchial sac, endostyle, CNS and siphons. Recent experiments suggest this source of pluripotent migratory progenitors, identified by expression of the Piwi protein, normally resides in the transverse vessels of the branchial sac.

IV.B. Piwi Expressing Cells (PECs) Accumulate in the OS

Progenitor plasticity varies widely across the few well-studied animal model organisms used to study regeneration. Primitive animals, such as *Hydra* and flatworms, contain migratory totipotent stem cells capable of regenerating any of the tissues present in the adult. However, the progenitor cells which contribute to salamander and zebrafish limb regeneration seem to be restricted to the germ-layer from which they are derived. Within the ascidians, some colonial species have been observed to contain circulatory

46

pluripotent stem cells derived from the vasculature; however, no analogous population has been definitively identified in solitary ascidians.

A feature common to all the aforementioned regenerative progenitor cell types is the expression of Piwi, a member of the argonaute family of RNA binding proteins. The Piwi protein functions in a variety of ways to restrict expression of other genes. Piwi has canonically been described as a germline stem cell and gonad tissue marker and is thought to play a role in maintaining genome integrity by repressing transposon transcription and preventing unwanted RNA translation. The protein typically localizes either within the nucleus or aggregates within extra-nuclear granules to perform these functions (e.g. stress granules, p-bodies and germline nuage). Recent experiments have also demonstrated a population of cells present in the transverse vessels of the adult *Ciona* branchial sac which also express Piwi, suggesting these cells may be progenitors which contribute to oral siphon regeneration.

Antibody staining for Piwi identified aggregates of Piwi expressing cells (PECs) present in un-amputated *Ciona* adults throughout the transverse vessels of the branchial sac (data not shown). During the time of approximately 24-72 hours following amputation, a large accumulation of PECs can be detected at the distal edge of regenerating OSs (Fig. 12E, F). Whether these cells migrate from the branchial sac following amputation or are simply cells that were already present at the site of amputation which are induced to express Piwi following injury remains unclear.

47
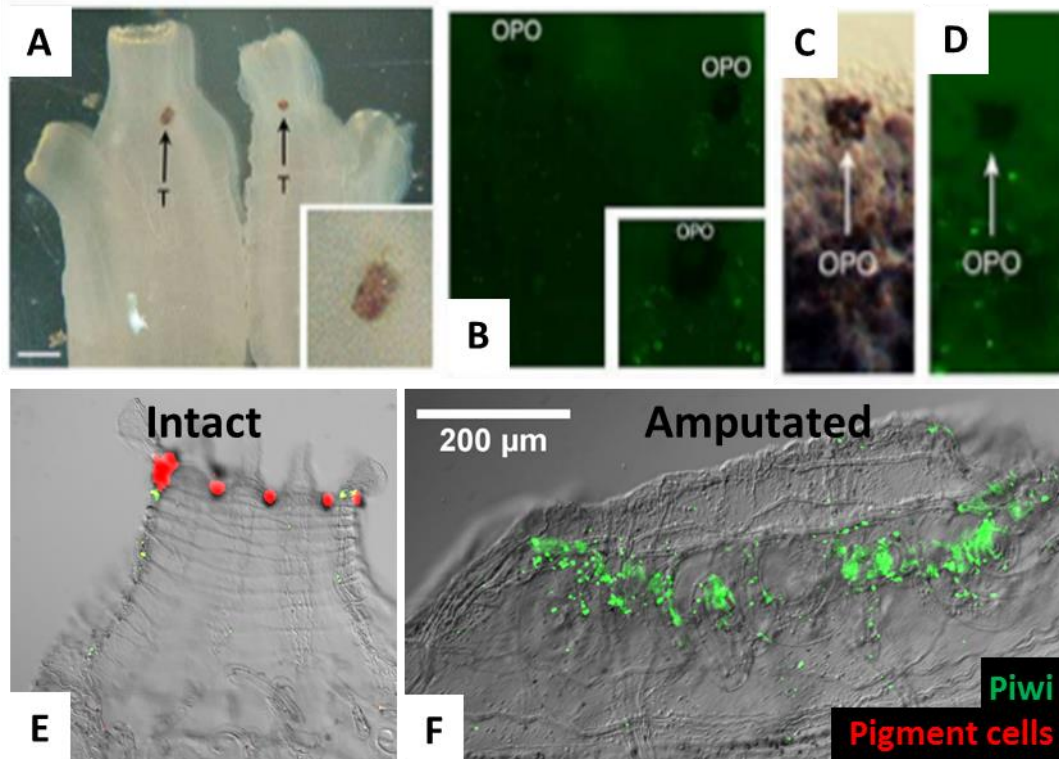
Figure 12. Piwi Expressing Cell Localization during Ciona OS Regeneration.
(A)−(D) Branchial sac transplantation experiments. (A) Hosts with neutral red stained donor branchial sac transplants (T). Scale bar is 3 mm. Inset: the left transplant in (E) magnified about 3×. (B) The oral siphon of a host with EdU labeled cells. Scale bar 50 μm. Inset: 2× magnification of (B) showing EdU labeled cells around the oral siphon pigmented organs (OPOs) in the regenerated host, (C, D) Bright field (C) and fluorescence (D) images of alkaline phosphatase stained and unlabeled OPOs in the 3 day regenerating oral siphon. Scale bar in (I) is 40 μm. (A-D) reproduced with permission from (Jeffery, 2015b). (E, F) An un-amputated (E) and D2 amputated OS (F) showing an accumulation of PECs at the distal edge of a regenerating OS. Overlay of DIC image with α-Piwi Ab staining in green, while auto-fluorescent pigment cells are shown in red.

Transplantation of EdU labeled branchial sac tissue into an unlabeled

recipient partially resolved this issue, when it was observed that a greater

number of transplanted cells (which are probably PECs) were found in the

OS of regenerating animals compared to un-amputated controls (Fig. 12A-D)

(Jeffery, 2015b). However, in those experiments the PECs themselves were

not labeled in any way, thus precluding strong conclusions about the

contributions of PECs to OS regeneration. If *Ciona* PECs normally migrate from the branchial sac and contribute to OS regeneration, the capacity in which they would be doing so remains unclear.

PECs could very well be pluripotent progenitors capable of differentiating into any of the cell types present in the adult OS. However, it's also possible the PECs in the branchial sac are lineage restricted, potentially even hematopoietic in origin and thus contribute to OS regeneration in only a limited manner. *Ciona* PECs could also be stimulatory, acting to coordinate re-patterning of the existing tissue present at the OS amputation site and/or inducing growth of lineage restricted progenitors present in the regenerating tissue. The ability of PECs to coordinate activity of cells already present at the amputation site is also supported by the partial UV irradiation experiments of Auger et al., (2010) (Fig 11A, B), which suggested some contribution of pre-existing OS cells to regeneration of new tissue. Additional work has been needed to characterize the extent to which PECs contribute to OS regeneration.

IV.C. PECs are Detectable in Circulation

Branchial sac transplantation experiments that demonstrated labeled PECs from the branchial sac are found in higher numbers in a regenerating OS did not address whether PECs are normally induced to migrate to the OS in the absence of branchial sac injury or to what extent there is an expansion in the circulating PEC population. In un-amputated *Ciona*, PECs can be

detected within the population of circulating blood cells. There are 8 previously described blood cell types in *Ciona,* two of these (hemoblasts and multinucleated) were observed to be positive for using antibody staining of blood smears on glass slides. Further, roughly 1% of the total blood cell population was identified to be PECs by FACS. The proportion of PECs increased to roughly 2% of the total blood cell population when analyzed by FACS at 2 days post-amputation (my unpublished data). This supports the hypothesis that branchial sac PECs are capable of migrating to the OS by traveling through the vasculature, however, it remained unclear if circulating PECs infiltrate regenerating OS tissue and whether they contribute to the regenerative process.

IV.D. Pharmacological Inhibition Disrupts OS Regeneration and PEC Expansion in the Branchial Sac

Functional analysis of RNAseq data from regenerating OS tissue showed enrichment of several categories associated with morphogenetic signaling pathways, suggesting a potential role in the coordination of progenitor cells (Fig. 7). I used pharmalogical inhibition to investigate the effect of disrupting key components in these signaling pathways on OS regeneration. Three drugs were selected for these experiments: 1) IWP-12, a Wnt pathway inhibitor, 2) FR180204, a selective ERK1/2 inhibitor, and 3) Praziquantel (PZQ) which is a calcium channel permeator used to treat parasitic schistosome infections but I discovered also has effects on OS regeneration.

All three drugs resulted in toxicity at 10µM when animals were treated for 5 successive days following amputation; however, continuous IWP-12 treatment at 5µM resulted in limited toxicity and partial inhibition of OS regeneration. Treatments were reduced to a 48 hour period following regeneration then optimized for an effective dose that did not cause a significant amount of toxicity (IWP-12 = 20µM, FR180204 = 20µM, PZQ = 50µM). All three of these treatments prevented OS regeneration by inhibiting tissue outgrowth.

I hypothesized these drugs could be preventing regeneration by either inhibiting proliferation and/or differentiation of progenitor cells. To address this I performed Piwi Ab staining on animals treated with each of the drugs for 48 hours following amputation. pSmad2/3 staining was used as a negative control and to investigate whether any possible interaction exists between the signaling pathway targeted by each drug and the TGF-ß pathway. All three drugs resulted in a decrease in the number of Piwi+ cells per unit area in the BS, but not the OS. Additionally, none of the drugs resulted in any effect on the number of pSmad2/3+ cells, indicating specificity for the Piwi+ subset of progenitor cells and supporting independence of the targeted signaling pathways from any potential interaction with TGF-ß signaling.

Table 5. ANOVA of Effect of Various Drugs on Piwi+ and pSmad2/3+ Cell Number in the Oral Siphon and Branchial Sac of Regenerating *Ciona*

Cohorts Analyzed	Treatment	P-Value	Interpretation
Piwi & pSmad2/3 cells in BS (n = 6)	FR vs. DMSO	0.154	Some effect in BS (overall)
	IWP vs. DMSO	0.058	
	PZQ vs. DMSO	0.187	
Piwi & pSmad2/3 cells in OS (n = 6)	FR vs. DMSO	0.9734	No effect in OS (overall)
	IWP vs. DMSO	0.999	
	PZQ vs. DMSO	0.999	
Piwi+ cells BS & OS (n = 6)	FR vs. DMSO	0.413	Some effects on Piwi+ cells (overall)
	IWP vs. DMSO	0.300	
	PZQ vs. DMSO	0.618	
pSmad2/3+ cells BS & OS (n = 6)	FR vs. DMSO	0.999	No effect on pSmad2/3+ cells (overall)
	IWP vs. DMSO	0.999	
	PZQ vs. DMSO	0.919	
Piwi+ cells in BS (n = 3)	FR vs. DMSO	0.362	Some effect on Piwi+ cells in BS
	IWP vs. DMSO	0.169	
	PZQ vs. DMSO	0.716	
pSmad2/3+ cells in BS (n=3)	FR vs. DMSO	0.998	No effect on pSmad2/3+ cells in BS
	IWP vs. DMSO	0.991	
	PZQ vs. DMSO	0.964	

V. Conclusions

Concurrent expression profiling of mRNA and miRNA has proven to be a useful approach for characterizing transcriptome wide changes in gene expression during OS regeneration. I successfully identified a variety of transcriptional changes supporting the hypothesis that several major features of vertebrate appendage regeneration are conserved in *Ciona*. Examples include categories of genes related to wound healing, proliferation, differentiation and ECM remodeling which were enriched at specific stages of regeneration. Further, I present a high confidence network of miRNAs and their predicted targets during OS regeneration. This enabled subsequent annotation of putative miRNA functions during regeneration by virtue of identifying discrete clusters of miRNAs and their associated targets within the network. Several clusters of miRNAs and their targets were found to significantly overlap with functional categories likely to be involved in specific stages of OS regeneration due to the preferential enrichment of functional categories at specific stages. This work provides a systematic characterization of mRNA and miRNA expression during OS regeneration, a comprehensive set of predicted interactions between these two gene product types and predicts effects of those interactions on cellular processes during regeneration; all are necessary to facilitate future investigation into the genetic requirements of appendage regeneration in chordates.

My work supports the predictions generated from my analysis of RNAseq data for OS regeneration by disrupting regeneration using several small-molecule pharmalogical inhibitors. However, effects predicted by gene expression changes in the OS resulted in changes in the BS population of PECs during pharmalogical treatments. This suggests circulating cells may normally be responding to signals from cells near the site of amputation within the OS, which then manifests in an expansion of the BS PEC population. This supports the hypothesis that the BS provides a niche for circulating PECs and that those PECs are essential for normal OS regeneration. However, my studies have not determined how PECs contribute to OS regeneration and in what capacity. Additional studies that track the lineage of PECs as they proliferate in the BS, then migrate through the circulatory system and ultimately interact with resident OS cells will be needed to determine whether PECs differentiate and assimilate into the regenerating OS.

VI. Materials and Methods

Animal Husbandry and RNA Extraction

C. robusta were collected at the Santa Barbara Yacht Harbor. Gametes from two adults were mixed and the resulting offspring were grown to approximately 6 months of age. Approximately 75 sibling animals ranging in size from 5-10 cm were selected for amputation and anesthetized in 0.04% MS222 for 30 min. Amputated siphon samples were immediately frozen in liquid nitrogen then transferred to 1 mL RNAlater-ICE (Life Technologies) and stored at -20°C for one week. Total RNA was extracted from a pool of five tissue samples for each replicate using the miRvana total RNA extraction kit (Life Technologies). During time-course experiments batches of animals were housed in five gallon buckets of seawater, changed daily and maintained at 15°C with a 12/12 hour artificial light/dark cycle.

RNA Sequencing and Data Pre-processing

PolyA+ RNA was isolated from 5 µg of total RNA using Dynabeads (Life Technologies). Small RNAs (approximately 18-30 bp), including miRNAs, were isolated from 1 µg of total RNA by 1% Tris/Borate/EDTA-Acrylamide gel electrophoresis. Sequencing libraries were prepared with the Total RNAseq Kit v2.0 (Life Technologies). Libraries were sequenced in multiplex using an Ion Proton sequencer from Life Technologies. Raw reads were trimmed of adapter sequences and pre-processed for base quality according to the default software

specifications. Further quality control was performed using FastQC and SamTools (Li et al., 2009). The *C. intestinalis* (now called *robusta*) JGI genome version 2.0 and Ensembl transcript models (release 83) were used as references for alignment. mRNA libraries were first aligned to the *C. robusta* genome and set of Ensemble transcript models using Tophat (Trapnell et al., 2009) with strict parameters ("end-to-end" mode) to accommodate spliced reads, then the initially unaligned reads were processed using Bowtie with relaxed parameters ("local" mode) to increase the overall robustness of alignment to the highly polymorphic *Ciona* genome. HTseq-count (Anders et al., 2015) was used to count reads for each mRNA transcript. microRNA precursor sequences were downloaded from miRBase (Kozomara and Griffiths-Jones, 2014) and used along with the *Ciona* genome by miRDeep2 (Friedländer et al., 2012) to align and quantify the miRNA libraries. Counts of novel miRNA's were extracted from the miRDeep2 output using a custom Python script.

Differential Expression, Co-expression and Enrichment Analyses

mRNA samples were initially normalized for sequencing depth and transcript length (RPKM, reads per kilobase per million) while miRNA samples were first normalized only by sequencing depth (CPM, counts per million). To reduce the number of tests performed, lowly and non-expressed genes were removed using filters of RPKM ≥ 5 or CPM ≥ 1 in at least three individual samples for mRNA and miRNA libraries, respectively. Normalization of counts and likelihood-ratio tests were performed with the EdgeR and DESeq2 packages

in R to determine differential expression relative to D0. Pairwise correlations (Pearson rho ≤ -0.9) were calculated using R from $\log_2$ fold-change values for mRNA and miRNA data sets estimated by DESeq2. To determine Gene Ontology categories and KEGG Pathways that were enriched at each stage relative to a reference stage (NR or D0), the mean $-\log_2$ transformed FDR adjusted p-value of each gene determined by EdgeR and DESeq2 was used as input for a two-tailed z-test (Maciejewski, 2013; Perez-Llamas and Lopez-Bigas, 2011). Z-tests were performed using a 10,000 replicate bootstrap and FDR multiple testing adjustment using Gitools 2.2.3 (Perez-Llamas and Lopez-Bigas, 2011). Significance of overlap between miRNA targets and functional categories was performed using hypergeometric tests in R, the resulting p-values were corrected for multiple testing (FDR). For overlap tests, lists or categories with fewer than 5 transcripts were removed to reduce false positives.

qRTPCR Validation of Relative Expression

Custom TaqMan assays manufactured by Thermo-Fisher were used for quantifying relative amounts of miRNA expression. SYBR green detection was used for quantifying relative amounts of mRNA expression. All experiments were performed using a QuantStudio 1200K-Flex platform and analyzed using Applied Biosciences ExpressionSuite software. mRNA expression levels were normalized to the geometric mean of GAPDH and RNA polymerase 2. Global normalization was used for miRNA expression levels because a sufficiently stable endogenous reference gene could not be identified despite testing several

of the least variable genes from the deep sequencing data. Primer sequences for

mRNA detection were designed using BatchPrimer3 (You et al., 2008) and are

listed in Table S5 of Spina et al., (2017) along with Ensembl transcript

identifiers and all gene names used in this study. The sequences of the miRNA

detection probes are proprietary and not available to the researchers. One-way

ANOVA was used to determine transcripts that were significantly DE during at

least one stage of regeneration by qRTPCR, results are shown in Table S6 of

Spina et al., 2017.

miRNA Target Prediction

3' UTR sequences and a paired list of orthologous genes for *C. robusta* and *C.

savignyi* were downloaded from Ensemble Biomart; then, orthologous 3'-UTR

sequences were then grouped according to the pairs of orthologous transcript

ID's. Each resulting group of orthologous 3'-UTRs was aligned using Clustal

Omega (Sievers et al., 2011) then the resulting alignments were concatenated

into a single file which included the remaining *C. robusta* 3'-UTRs that did not

have orthologs in *C. savignyi*. The multiple alignment results were used with

mature microRNA sequences downloaded from miRBase directly by

TargetScanS (Lewis et al., 2005) to identify conserved seed regions for all *Ciona*

miRNAs (known and predicted in this study).

References

Agarwal, V., Bell, G.W., Nam, J.-W., and Bartel, D.P. (2015). Predicting effective microRNA target sites in mammalian mRNAs. eLife *4*, e05005.

Albert, R. (2005). Scale-free networks in cell biology. J. Cell Sci. *118*, 4947–4957.

Alvarado, A.S., and Tsonis, P.A. (2006). Bridging the regeneration gap: genetic insights from diverse animal models. Nat. Rev. Genet. *7*, 873–884.

Arpino, V., Brock, M., and Gill, S.E. (2015). The role of TIMPs in regulation of extracellular matrix proteolysis. Matrix Biol. *44–46*, 247–254.

Ashburner, M., Ball, C.A., Blake, J.A., Botstein, D., Butler, H., Cherry, J.M., Davis, A.P., Dolinski, K., Dwight, S.S., Eppig, J.T., et al. (2000). Gene Ontology: tool for the unification of biology. Nat. Genet. *25*, 25–29.

Auger, H., Sasakura, Y., Joly, J.-S., and Jeffery, W.R. (2010). Regeneration of oral siphon pigment organs in the ascidian Ciona intestinalis. Dev. Biol. *339*, 374–389.

Barabási, A.-L., and Oltvai, Z.N. (2004). Network biology: understanding the cell's functional organization. Nat. Rev. Genet. *5*, 101–113.

Barker, N. (2014). Adult intestinal stem cells: critical drivers of epithelial homeostasis and regeneration. Nat. Rev. Mol. Cell Biol. *15*, 19–33.

Barker, N., Wetering, M. van de, and Clevers, H. (2008). The intestinal stem cell. Genes Dev. *22*, 1856–1864.

Bely, A.E., and Nyberg, K.G. (2010). Evolution of animal regeneration: re-emergence of a field. Trends Ecol. Evol. *25*, 161–170.

Bonev, B., Stanley, P., and Papalopulu, N. (2012). MicroRNA-9 Modulates Hes1 Ultradian Oscillations by Forming a Double-Negative Feedback Loop. Cell Rep. *2*, 10–18.

Brown, F.D., Keeling, E.L., Le, A.D., and Swalla, B.J. (2009). Whole body regeneration in a colonial ascidian, Botrylloides violaceus. J. Exp. Zoolog. B Mol. Dev. Evol. *312*, 885–900.

Brunetti, R., Gissi, C., Pennati, R., Caicci, F., Gasparini, F., and Manni, L. (2015). Morphological evidence that the molecularly determined Ciona intestinalis type A and type B are different species: Ciona robusta and Ciona intestinalis. J. Zool. Syst. Evol. Res. *53*, 186–193.

Busby, M.A., Stewart, C., Miller, C.A., Grzeda, K.R., and Marth, G.T. (2013). Scotty: a web tool for designing RNA-Seq experiments to measure differential gene expression. Bioinformatics *29*, 656–657.

Calve, S., Odelberg, S.J., and Simon, H.-G. (2010). A Transitional Extracellular Matrix Instructs Cell Behavior During Muscle Regeneration. Dev. Biol. *344*, 259–271.

Campbell, L.J., Suárez-Castillo, E.C., Ortiz-Zuazaga, H., Knapp, D., Tanaka, E.M., and Crews, C.M. (2011). Gene expression profile of the regeneration epithelium during axolotl limb regeneration. Dev. Dyn. *240*, 1826–1840.

Carthew, R.W., and Sontheimer, E.J. (2009). Origins and Mechanisms of miRNAs and siRNAs. Cell *136*, 642–655.

Chablais, F., and Jazwinska, A. (2010). IGF signaling between blastema and wound epidermis is required for fin regeneration. Dev. Camb. Engl. *137*, 871–879.

Chen, J.S., Pedro, M.S., and Zeller, R.W. (2011). miR-124 function during Ciona intestinalis neuronal development includes extensive interaction with the Notch signaling pathway. Development *138*, 4943–4953.

Chiba, S., Sasaki, A., Nakayama, A., Takamura, K., and Satoh, N. (2004). Development of Ciona intestinalis Juveniles (Through 2nd Ascidian Stage). Zoolog. Sci. *21*, 285–298.

Chou, C.-H., Chang, N.-W., Shrestha, S., Hsu, S.-D., Lin, Y.-L., Lee, W.-H., Yang, C.-D., Hong, H.-C., Wei, T.-Y., Tu, S.-J., et al. (2016). miRTarBase 2016: updates to the experimentally validated miRNA-target interactions database. Nucleic Acids Res. *44*, D239–D247.

Coolen, M., Katz, S., and Bally-Cuif, L. (2013). miR-9: a versatile regulator of neurogenesis. Front. Cell. Neurosci. *7*, 220.

Crow, K.D., and Wagner, G.P. (2006). What Is the Role of Genome Duplication in the Evolution of Complexity and Diversity? Mol. Biol. Evol. *23*, 887–892.

Dahlberg, C., Auger, H., Dupont, S., Sasakura, Y., Thorndyke, M., and Joly, J.-S. (2009). Refining the Ciona intestinalis Model of Central Nervous System Regeneration. PLOS ONE *4*, e4458.

Dehal, P., and Boore, J.L. (2005). Two Rounds of Whole Genome Duplication in the Ancestral Vertebrate. PLOS Biol *3*, e314.

Dehal, P., Satou, Y., Campbell, R.K., Chapman, J., Degnan, B., Tomaso, A.D., Davidson, B., Gregorio, A.D., Gelpke, M., Goodstein, D.M., et al. (2002). The Draft Genome of Ciona intestinalis: Insights into Chordate and Vertebrate Origins. Science *298*, 2157–2167.

Delsuc, F., Brinkmann, H., Chourrout, D., and Philippe, H. (2006). Tunicates and not cephalochordates are the closest living relatives of vertebrates. Nature *439*, 965–968.

Endo, T., Bryant, S.V., and Gardiner, D.M. (2004). A stepwise model system for limb regeneration. Dev. Biol. *270*, 135–145.

Friedländer, M.R., Mackowiak, S.D., Li, N., Chen, W., and Rajewsky, N. (2012). miRDeep2 accurately identifies known and hundreds of novel microRNA genes in seven animal clades. Nucleic Acids Res. *40*, 37–52.

Galderisi, U., Jori, F.P., and Giordano, A. (2003). Cell cycle regulation and neural differentiation. Oncogene *22*, 5208–5219.

Galliot, B., and Ghila, L. (2010). Cell plasticity in homeostasis and regeneration. Mol. Reprod. Dev. *77*, 837–855.

Gearhart, M.D., Erickson, J.R., Walsh, A., and Echeverri, K. (2015). Identification of Conserved and Novel MicroRNAs during Tail Regeneration in the Mexican Axolotl. Int. J. Mol. Sci. *16*, 22046–22061.

Geng, J., Gates, P.B., Kumar, A., Guenther, S., Garza-Garcia, A., Kuenne, C., Zhang, P., Looso, M., and Brockes, J.P. (2015). Identification of the orphan gene Prod 1 in basal and other salamander families. EvoDevo *6*, 9.

Gilbert, R.W.D., Vickaryous, M.K., and Viloria-Petit, A.M. (2013). Characterization of TGFβ signaling during tail regeneration in the leopard Gecko (Eublepharis macularius). Dev. Dyn. *242*, 886–896.

Godwin, J.W., Pinto, A.R., and Rosenthal, N.A. (2013). Macrophages are required for adult salamander limb regeneration. Proc. Natl. Acad. Sci. *110*, 9415–9420.

Griffiths-Jones, S. (2004). The microRNA Registry. Nucleic Acids Res. *32*, D109–D111.

Guedelhoefer, O.C., and Sánchez Alvarado, A. (2012). Amputation induces stem cell mobilization to sites of injury during planarian regeneration. Dev. Camb. Engl. *139*, 3510–3520.

Hamada, M., Goricki, S., Byerly, M.S., Satoh, N., and Jeffery, W.R. (2015a). Evolution of the chordate regeneration blastema: Differential gene expression and conserved role of notch signaling during siphon regeneration in the ascidian Ciona. Dev. Biol. *405*, 304–315.

Harty, M., Neff, A.W., King, M.W., and Mescher, A.L. (2003). Regeneration or scarring: An immunologic perspective. Dev. Dyn. *226*, 268–279.

Hendrix, D., Levine, M., and Shi, W. (2010). miRTRAP, a computational method for the systematic identification of miRNAs from high throughput sequencing data. Genome Biol. *11*, R39.

Ho, D.M., and Whitman, M. (2008). TGF-beta signaling is required for multiple processes during Xenopus tail regeneration. Dev. Biol. *315*, 203–216.

Holman, E.C., Campbell, L.J., Hines, J., and Crews, C.M. (2012). Microarray Analysis of microRNA Expression during Axolotl Limb Regeneration. PLOS ONE *7*, e41804.

Huang, K., and Fan, G. (2010). DNA methylation in cell differentiation and reprogramming: an emerging systematic view. Regen. Med. *5*, 531–544.

Hutchins, E.D., Eckalbar, W.L., Wolter, J.M., Mangone, M., and Kusumi, K. (2016). Differential expression of conserved and novel microRNAs during tail regeneration in the lizard Anolis carolinensis. BMC Genomics *17*, 339.

Hwa, V., Oh, Y., and Rosenfeld, R.G. (1999). The insulin-like growth factor-binding protein (IGFBP) superfamily. Endocr. Rev. *20*, 761–787.

Jeffery, W.R. (2012). Siphon regeneration capacity is compromised during aging in the ascidian Ciona intestinalis. Mech. Ageing Dev. *133*, 629–636.

Jeffery, W.R. (2015a). Closing the wounds: One hundred and twenty five years of regenerative biology in the ascidian Ciona intestinalis. Genesis *53*, 48–65.

Jeffery, W.R. (2015b). Distal Regeneration Involves the Age Dependent Activity of Branchial Sac Stem Cells in the Ascidian Ciona intestinalis. Regeneration *2*, 1–18.

Jhamb, D., Rao, N., Milner, D.J., Song, F., Cameron, J.A., Stocum, D.L., and Palakal, M.J. (2011). Network based transcription factor analysis of regenerating axolotl limbs. BMC Bioinformatics *12*, 80.

Jing, L., Jia, Y., Lu, J., Han, R., Li, J., Wang, S., Peng, T., and Jia, Y. (2011). MicroRNA-9 promotes differentiation of mouse bone mesenchymal stem cells into neurons by Notch signaling: NeuroReport *22*, 206–211.

Juliano, C., and Wessel, G. (2010). Versatile Germline Genes. Science *329*, 640–641.

Juliano, C., Wang, J., and Lin, H. (2011). Uniting germline and stem cells: the function of Piwi proteins and the piRNA pathway in diverse organisms. Annu. Rev. Genet. *45*, 447–469.

Kanehisa, M., and Goto, S. (2000). KEGG: kyoto encyclopedia of genes and genomes. Nucleic Acids Res. *28*, 27–30.

Keshavan, R., Virata, M., Keshavan, A., and Zeller, R.W. (2010). Computational identification of Ciona intestinalis microRNAs. Zoolog. Sci. *27*, 162–170.

King, R.S., and Newmark, P.A. (2012). The cell biology of regeneration. J. Cell Biol. *196*, 553–562.

Knapp, D., Schulz, H., Rascon, C.A., Volkmer, M., Scholz, J., Nacu, E., Le, M., Novozhilov, S., Tazaki, A., Protze, S., et al. (2013). Comparative Transcriptional Profiling of the Axolotl Limb Identifies a Tripartite Regeneration-Specific Gene Program. PLOS ONE *8*, e61352.

Kourakis, M.J., and Smith, W.C. (2007). A conserved role for FGF signaling in chordate otic/atrial placode formation. Dev. Biol. *312*, 245–257.

Kovács, I.A., Palotai, R., Szalay, M.S., and Csermely, P. (2010). Community Landscapes: An Integrative Approach to Determine Overlapping Network Module Hierarchy, Identify Key Nodes and Predict Network Dynamics. PLOS ONE *5*, e12528.

Kozomara, A., and Griffiths-Jones, S. (2014). miRBase: annotating high confidence microRNAs using deep sequencing data. Nucleic Acids Res. *42*, D68–D73.

Kragl, M., Knapp, D., Nacu, E., Khattak, S., Maden, M., Epperlein, H.H., and Tanaka, E.M. (2009). Cells keep a memory of their tissue origin during axolotl limb regeneration. Nature *460*, 60–65.

Kuang, Y., Liu, Q., Shu, X., Zhang, C., Huang, N., Li, J., Jiang, M., and Li, H. (2012). Dicer1 and MiR-9 are required for proper Notch1 signaling and the Bergmann glial phenotype in the developing mouse cerebellum. Glia *60*, 1734–1746.

Kumar, A., and Brockes, J.P. (2012). Nerve dependence in tissue, organ, and appendage regeneration. Trends Neurosci. *35*, 691–699.

Kürn, U., Rendulic, S., Tiozzo, S., and Lauzon, R.J. (2011). Asexual Propagation and Regeneration in Colonial Ascidians. Biol. Bull. *221*, 43–61.

Kusakabe, R., Tani, S., Nishitsuji, K., Shindo, M., Okamura, K., Miyamoto, Y., Nakai, K., Suzuki, Y., Kusakabe, T.G., and Inoue, K. (2013). Characterization of the compact bicistronic microRNA precursor, miR-1/miR-133, expressed specifically in Ciona muscle tissues. Gene Expr. Patterns *13*, 43–50.

Lane, S.W., Williams, D.A., and Watt, F.M. (2014). Modulating the stem cell niche for tissue regeneration. Nat. Biotechnol. *32*, 795–803.

Lévesque, M., Gatien, S., Finnson, K., Desmeules, S., Villiard, É., Pilote, M., Philip, A., and Roy, S. (2007). Transforming Growth Factor: β Signaling Is Essential for Limb Regeneration in Axolotls. PLOS ONE *2*, e1227.

Lewis, B.P., Burge, C.B., and Bartel, D.P. (2005). Conserved seed pairing, often flanked by adenosines, indicates that thousands of human genes are microRNA targets. Cell *120*, 15–20.

Love, M.I., Huber, W., and Anders, S. (2014a). Moderated estimation of fold change and dispersion for RNA-seq data with DESeq2. Genome Biol. *15*.

Love, N.R., Chen, Y., Bonev, B., Gilchrist, M.J., Fairclough, L., Lea, R., Mohun, T.J., Paredes, R., Zeef, L.A., and Amaya, E. (2011). Genome-wide analysis of gene expression during Xenopus tropicalis tadpole tail regeneration. BMC Dev. Biol. *11*, 70.

Love, N.R., Ziegler, M., Chen, Y., and Amaya, E. (2014b). Carbohydrate metabolism during vertebrate appendage regeneration: What is its role? How is it regulated?: A postulation that regenerating vertebrate appendages facilitate glycolytic and pentose phosphate pathways to fuel macromolecule biosynthesis. Bioessays *36*, 27–33.

Lu, P., Takai, K., Weaver, V.M., and Werb, Z. (2011). Extracellular Matrix Degradation and Remodeling in Development and Disease. Cold Spring Harb. Perspect. Biol. *3*.

Maienschein, J. (2011). Regenerative medicine's historical roots in regeneration, transplantation, and translation. Dev. Biol. *358*, 278–284.

McBeath, R., Pirone, D.M., Nelson, C.M., Bhadriraju, K., and Chen, C.S. (2004). Cell Shape, Cytoskeletal Tension, and RhoA Regulate Stem Cell Lineage Commitment. Dev. Cell *6*, 483–495.

McCusker, C., Bryant, S.V., and Gardiner, D.M. (2015). The axolotl limb blastema: cellular and molecular mechanisms driving blastema formation and limb regeneration in tetrapods. Regeneration *2*, 54–71.

Messerschmidt, D.M., Knowles, B.B., and Solter, D. (2014). DNA methylation dynamics during epigenetic reprogramming in the germline and preimplantation embryos. Genes Dev. *28*, 812–828.

Missal, K., Rose, D., and Stadler, P.F. (2005). Non-coding RNAs in Ciona intestinalis. Bioinforma. Oxf. Engl. *21 Suppl 2*, ii77-78.

Mita, K., and Fujiwara, S. (2007). Nodal regulates neural tube formation in the Ciona intestinalis embryo. Dev. Genes Evol. *217*, 593–601.

Mitchelson, K.R., and Qin, W.-Y. (2015). Roles of the canonical myomiRs miR-1, -133 and -206 in cell development and disease. World J. Biol. Chem. *6*, 162–208.

Monaghan, J.R., Epp, L.G., Putta, S., Page, R.B., Walker, J.A., Beachy, C.K., Zhu, W., Pao, G.M., Verma, I.M., Hunter, T., et al. (2009). Microarray and cDNA sequence analysis of transcription during nerve-dependent limb regeneration. BMC Biol. *7*, 1.

Murawala, P., Tanaka, E.M., and Currie, J.D. (2012). Regeneration: The ultimate example of wound healing. Semin. Cell Dev. Biol. *23*, 954–962.

Nishida, H., and Sawada, K. (2001). macho-1 encodes a localized mRNA in ascidian eggs that specifies muscle fate during embryogenesis. Nature *409*, 724–729.

Norden-Krichmar, T.M., Holtz, J., Pasquinelli, A.E., and Gaasterland, T. (2007). Computational prediction and experimental validation of Ciona intestinalis microRNA genes. BMC Genomics *8*, 445.

O'Connor, M.D., Kardel, M.D., Iosfina, I., Youssef, D., Lu, M., Li, M.M., Vercauteren, S., Nagy, A., and Eaves, C.J. (2008). Alkaline phosphatase-positive colony formation is a sensitive, specific, and quantitative indicator of undifferentiated human embryonic stem cells. Stem Cells Dayt. Ohio *26*, 1109–1116.

Odelberg, S.J. (2004). Unraveling the Molecular Basis for Regenerative Cellular Plasticity. PLoS Biol. *2*.

Osugi, T., Sasakura, Y., and Satake, H. (2017). The nervous system of the adult ascidian Ciona intestinalis Type A (Ciona robusta): Insights from transgenic animal models. PLOS ONE *12*, e0180227.

Pfefferli, C., and Jaźwińska, A. (2015). The art of fin regeneration in zebrafish. Regeneration *2*, 72–83.

Rao, N., Jhamb, D., Milner, D.J., Li, B., Song, F., Wang, M., Voss, S.R., Palakal, M., King, M.W., Saranjami, B., et al. (2009). Proteomic analysis of blastema formation in regenerating axolotl limbs. BMC Biol. *7*, 83.

Reddien, P.W., and Sánchez Alvarado, A. (2004). Fundamentals of planarian regeneration. Annu. Rev. Cell Dev. Biol. *20*, 725–757.

Rinkevich, B., Shlemberg, Z., and Fishelson, L. (1995). Whole-body protochordate regeneration from totipotent blood cells. Proc. Natl. Acad. Sci. U. S. A. *92*, 7695–7699.

Rinkevich, Y., Rosner, A., Rabinowitz, C., Lapidot, Z., Moiseeva, E., and Rinkevich, B. (2010). Piwi positive cells that line the vasculature epithelium, underlie whole body regeneration in a basal chordate. Dev. Biol. *345*, 94–104.

Rinkevich, Y., Voskoboynik, A., Rosner, A., Rabinowitz, C., Paz, G., Oren, M., Douek, J., Alfassi, G., Moiseeva, E., Ishizuka, K.J., et al. (2013). Repeated, long-term cycling of putative stem cells between niches in a basal chordate. Dev. Cell *24*.

Robles, J.A., Qureshi, S.E., Stephen, S.J., Wilson, S.R., Burden, C.J., and Taylor, J.M. (2012). Efficient experimental design and analysis strategies for the detection of differential expression using RNA-Sequencing. BMC Genomics *13*, 484.

Satoh, A., Bryant, S.V., and Gardiner, D.M. (2008). Regulation of dermal fibroblast dedifferentiation and redifferentiation during wound healing and limb regeneration in the Axolotl. Dev. Growth Differ. *50*, 743–754.

Satou, Y., Mineta, K., Ogasawara, M., Sasakura, Y., Shoguchi, E., Ueno, K., Yamada, L., Matsumoto, J., Wasserscheid, J., Dewar, K., et al. (2008). Improved genome assembly and evidence-based global gene model set for the chordate Ciona intestinalis: new insight into intron and operon populations. Genome Biol. *9*, R152.

Schebesta, M., Lien, C.-L., Engel, F.B., and Keating, M.T. (2006). Transcriptional profiling of caudal fin regeneration in zebrafish. ScientificWorldJournal *6 Suppl 1*, 38–54.

Seifert, A.W., Kiama, S.G., Seifert, M.G., Goheen, J.R., Palmer, T.M., and Maden, M. (2012). Skin shedding and tissue regeneration in African spiny mice (Acomys). Nature *489*, 561–565.

Sen, C.K., and Ghatak, S. (2015). miRNA control of tissue repair and regeneration. Am. J. Pathol. *185*, 2629–2640.

Shi, W., Hendrix, D., Levine, M., and Haley, B. (2009). A distinct class of small RNAs arises from pre-miRNA-proximal regions in a simple chordate. Nat. Struct. Mol. Biol. *16*, 183–189.

Shirae-Kurabayashi, M., Nishikata, T., Takamura, K., Tanaka, K.J., Nakamoto, C., and Nakamura, A. (2006). Dynamic redistribution of vasa homolog and exclusion of somatic cell determinants during germ cell specification in Ciona intestinalis. Dev. Camb. Engl. *133*, 2683–2693.

Shirae-Kurabayashi, M., Matsuda, K., and Nakamura, A. (2011). Ci-Pem-1 localizes to the nucleus and represses somatic gene transcription in the germline of Ciona intestinalis embryos. Dev. Camb. Engl. *138*, 2871–2881.

da Silva, S.M., Gates, P.B., and Brockes, J.P. (2002). The Newt Ortholog of CD59 Is Implicated in Proximodistal Identity during Amphibian Limb Regeneration. Dev. Cell *3*, 547–555.

Simone, T.M., Higgins, C.E., Czekay, R.-P., Law, B.K., Higgins, S.P., Archambeault, J., Kutz, S.M., and Higgins, P.J. (2014). SERPINE1: A Molecular Switch in the Proliferation-Migration Dichotomy in Wound-"Activated" Keratinocytes. Adv. Wound Care *3*, 281–290.

Smoot, M.E., Ono, K., Ruscheinski, J., Wang, P.-L., and Ideker, T. (2011). Cytoscape 2.8: new features for data integration and network visualization. Bioinformatics *27*, 431–432.

Spina, E.J., Guzman, E., Zhou, H., Kosik, K.S., and Smith, W.C. (2017). A microRNA-mRNA expression network during oral siphon regeneration in Ciona. Dev. Camb. Engl. *144*, 1787–1797.

Štefková, K., Procházková, J., and Pacherník, J. (2015). Alkaline Phosphatase in Stem Cells, Alkaline Phosphatase in Stem Cells. Stem Cells Int. Stem Cells Int. *2015*, *2015*, e628368.

Stewart, R., Rascón, C.A., Tian, S., Nie, J., Barry, C., Chu, L.-F., Ardalani, H., Wagner, R.J., Probasco, M.D., Bolin, J.M., et al. (2013). Comparative RNA-seq Analysis in the Unsequenced Axolotl: The Oncogene Burst Highlights Early Gene Expression in the Blastema. PLOS Comput Biol *9*, e1002936.

Stoick-Cooper, C.L., Moon, R.T., and Weidinger, G. (2007). Advances in signaling in vertebrate regeneration as a prelude to regenerative medicine. Genes Dev. *21*, 1292–1315.

Szalay-Bekő, M., Palotai, R., Szappanos, B., Kovács, I.A., Papp, B., and Csermely, P. (2012). ModuLand plug-in for Cytoscape: determination of hierarchical layers of overlapping network modules and community centrality. Bioinformatics *28*, 2202–2204.

Tan, S.-L., Ohtsuka, T., González, A., and Kageyama, R. (2012). MicroRNA9 regulates neural stem cell differentiation by controlling Hes1 expression dynamics in the developing brain. Genes Cells *17*, 952–961.

Terai, G., Okida, H., Asai, K., and Mituyama, T. (2012). Prediction of Conserved Precursors of miRNAs and Their Mature Forms by Integrating Position-Specific Structural Features. PLOS ONE *7*, e44314.

Thatcher, E.J., Paydar, I., Anderson, K.K., and Patton, J.G. (2008). Regulation of zebrafish fin regeneration by microRNAs. Proc. Natl. Acad. Sci. *105*, 18384–18389.

Tiozzo, S., and Copley, R.R. (2015). Reconsidering regeneration in metazoans: an evo-devo approach. Evol. Dev. Biol. *3*, 67.

Vander Heiden, M.G., Cantley, L.C., and Thompson, C.B. (2009). Understanding the Warburg Effect: The Metabolic Requirements of Cell Proliferation. Science *324*, 1029–1033.

Veeman, M.T., Newman-Smith, E., El-Nachef, D., and Smith, W.C. (2010). The ascidian mouth opening is derived from the anterior neuropore: reassessing the mouth/neural tube relationship in chordate evolution. Dev. Biol. *344*, 138–149.

Venuti, J.M., and Jeffery, W.R. (1989). Cell lineage and determination of cell fate in ascidian embryos. Int. J. Dev. Biol. *33*, 197–212.

Vethamany-Globus, S. (1987). Hormone action in newt limb regeneration: insulin and endorphins. Biochem. Cell Biol. Biochim. Biol. Cell. *65*, 730–738.

Vogt, G. (2012). Hidden Treasures in Stem Cells of Indeterminately Growing Bilaterian Invertebrates. Stem Cell Rev. Rep. *8*, 305–317.

Voskoboynik, A., Simon-Blecher, N., Soen, Y., Rinkevich, B., Tomaso, A.W.D., Ishizuka, K.J., and Weissman, I.L. (2007). Striving for normality: whole body regeneration through a series of abnormal generations. FASEB J. *21*, 1335–1344.

Wagner, D.E., Wang, I.E., and Reddien, P.W. (2011). Clonogenic Neoblasts Are Pluripotent Adult Stem Cells That Underlie Planarian Regeneration. Science *332*, 811–816.

Weissman, I.L. (2000). Stem cells: units of development, units of regeneration, and units in evolution. Cell *100*, 157–168.

Whyte, J.L., Smith, A.A., and Helms, J.A. (2012). Wnt Signaling and Injury Repair. Cold Spring Harb. Perspect. Biol. *4*.

Wolf, Y.I., Karev, G., and Koonin, E.V. (2002). Scale-free networks in biology: new insights into the fundamentals of evolution?*. BioEssays *24*, 105–109.

Wu, C.-H., Tsai, M.-H., Ho, C.-C., Chen, C.-Y., and Lee, H.-S. (2013). De novo transcriptome sequencing of axolotl blastema for identification of differentially expressed genes during limb regeneration. BMC Genomics *14*, 434.

Yin, V.P., Thomson, J.M., Thummel, R., Hyde, D.R., Hammond, S.M., and Poss, K.D. (2008). Fgf-dependent depletion of microRNA-133 promotes appendage regeneration in zebrafish. Genes Dev. *22*, 728–733.

Zondag, L.E., Rutherford, K., Gemmell, N.J., and Wilson, M.J. (2016). Uncovering the pathways underlying whole body regeneration in a chordate model, Botrylloides leachi using de novo transcriptome analysis. BMC Genomics *17*, 114.

Appendix

Transcript Names and Primer Sequences Used in this Study. All transcript names used in the primary text are listed here with the corresponding Ensembl transcript identifier, a description of the transcript and primer sequences used for qRTPCR validation, if applicable.

Name	Description	ID	Forward Primer	Reverse Primer
Caspase-2-like	Caspase-2-like	ENSCINT00000002830	ATGACGTGCTTGCATTGTTC	CGACCCACCTCAGTAAGCAT
FIBCD1a	Fibrinogen C domain containing 1	ENSCINT00000003420	GAAACCGAACTGGTCGAAAG	CCGGATACAGCAAGTGCATA
Rev-erb	Rev-erb	ENSCINT00000004784	GTCGAATCCCAAAGAAGCAG	GTGTTTCTTGCACCGTTTGA
TNFR-associated	TNF receptor-associated factor 3-like	ENSCINT00000005981	ATGGGCTATGTTGGATGGAA	CAATCTGCTGCTCAAATCCA
Tolloid	Tolloid	ENSCINT00000007799	GTAAAGAAGCCGGGTGTGAG	CTGTTGTATGCGAGGCAGAA
HSP70	Heat shock protein 70	ENSCINT00000011757	TGATAAACGAACCCACAGCA	ATCCAACTCGACAGCAGCTT
HB3	Non-symbiotic hemoglobin 3	ENSCINT00000013341	TGAGTAACGTTGGACTTGCTG	CCCAAGCTTGCATTACTGGT
Tomo-regulin	Tomoregulin-1-like	ENSCINT00000016852	TGCTTGGATGAAGTTGATGG	CATGCGACTGTAACGATTCC
Prospero	Prospero homeobox protein	ENSCINT00000018262	GCACCTCAGCATTACCCAAT	TTGGTCACGACGTCAAGAAA
FIBCD1b	Fibrinogen C domain containing 1	ENSCINT00000019098	GAAACCGAACTGGTCGAAAG	CCGGATACAGCAAGTGCATA
DIAP2	Drosophila Inhibitor of Apoptosis 2	ENSCINT00000020067	TTGCAAGCACCCATATACGA	GATGTGGATGGTTTGGGAGT
bZIP	CCAAT/Enhancer Binding Protein	ENSCINT00000023320	CGCTCGTACTCAAGCAACAG	ACAACATCATGGGACGGATT
TLR2	Toll-like receptor 2	ENSCINT00000024647	CAGTGATTCCGATGATGTGG	GGTGCTTGGATGGCAGTAAT
TNFR	Tumor Necrosis Factor Receptor	ENSCINT00000026302	GAAGATGCGTCCCATGCTAT	GAATGCCATGGACATCACAG
NEK11-like	NIMA related kinase 11-like	ENSCINT00000026775	GAATATTGTGAGGGCGGAGA	ACAACACCAAGGGACCAAAG
Matrillin	VWF domain containing protein	ENSCINT00000027938	CGTAAAGGAATGGGTGAAGC	TGAATGACATCCGGCAAGTA
Laminin subunit beta 2	EGF domain containing protein	ENSCINT00000031265	TTTCTTCTTTGGCGATGCTT	TCAGCGCTTCTTCTCACGTA
IGF-like	Insulin-like 3 protein	ENSCINT00000031399	CTGGAACGAAGTGCAAAGGT	TATTGCCATGCAGGTAACGA
DBX1-A	Hlx Homebox protein DBX1-A	ENSCINT00000033135	TCAGTCCAACCTATGCACCA	AGGGTAAGATGGGTGTGACG
Hsp90	Heat shock protein 90	ENSCINT00000035165	TAGCCGCCACACATGTTAAA	GCAGCAAGAGCTGCATCAT

Collagen, type XIV, alpha 1	VWF domain containing protein	ENSCINT00000036027	CGATCGCTCACGTAACAAAC	TTCCTGCAGTGTGTAGGCTCT
EMX	EMX Homeobox	ENSCINT00000037147	CCACCAGGATTCCAACAAAC	TCAGCTCCAACCACGTAATG
IGFbp	MAC25-like	ENSCINT00000037260	TTCATTTGGTAGGTGCGTGA	TATTCACACGATGCGGAAGA
Villin-1	Villin-1	ENSCINT00000003800		
SFI1-like	SFI1-like	ENSCINT00000008827		
Sideroflexin-1-like	Sideroflexin-1-like	ENSCINT00000010013		
NEK7-like	NIMA related kinase 7-like	ENSCINT00000017101		
Ubiquilin-1	Ubiquilin-1	ENSCINT00000017880		
MYBB1A	MYB Binding 1A	ENSCINT00000018013		
LIMK1-like	LIM Kinase 1 Like	ENSCINT00000024269		
Myosin X	PH domain containing protein	ENSCINT00000033884		
Kinesin	Kinesin	ENSCINT00000035420		
LMNTD1	Lamin tail domain containing 1	ENSCINT00000036416		

LIST OF TABLES